Coupled Ocean–Atmosphere Dynamical Processes in the Tropical Indian and Pacific Oceans and the TBO

GERALD A. MEEHL, JULIE M. ARBLASTER, AND JOHANNES LOSCHNIGG*

National Center for Atmospheric Research,+ Boulder, Colorado

(Manuscript received 6 May 2002, in final form 1 January 2003)

ABSTRACT

The transitions (from relatively strong to relatively weak monsoon) in the tropospheric biennial oscillation (TBO) occur in northern spring for the south Asian or Indian monsoon and northern fall for the Australian monsoon involving coupled land–atmosphere–ocean processes over a large area of the Indo-Pacific region. Transitions from March–May (MAM) to June–September (JJAS) tend to set the system for the next year, with a transition to the opposite sign the following year. Previous analyses of observed data and GCM sensitivity experiments have demonstrated that the TBO (with roughly a 2–3-yr period) encompasses most ENSO years (with their well-known biennial tendency). In addition, there are other years, including many Indian Ocean dipole (or zonal mode) events, that contribute to biennial transitions. Results presented here from observations for composites of TBO evolution confirm earlier results that the Indian and Pacific SST forcings are more dominant in the TBO than circulation and meridional temperature gradient anomalies over Asia. A fundamental element of the TBO is the large-scale east–west atmospheric circulation (the Walker circulation) that links anomalous convection and precipitation, winds, and ocean dynamics across the Indian and Pacific sectors. This circulation connects convection over the Asian–Australian monsoon regions both to the central and eastern Pacific (the eastern Walker cell), and to the central and western Indian Ocean (the western Walker cell). Analyses of upper-ocean data confirm previous results and show that ENSO El Niño and La Niña events as well as Indian Ocean SST dipole (or zonal mode) events are often large-amplitude excursions of the TBO in the tropical Pacific and Indian Oceans, respectively, associated with anomalous eastern and western Walker cell circulations, coupled ocean dynamics, and upper-ocean temperature and heat content anomalies. Other years with similar but lower-amplitude signals in the tropical Pacific and Indian Oceans also contribute to the TBO. Observed upper-ocean data for the Indian Ocean show that slowly eastward-propagating equatorial ocean heat content anomalies, westward-propagating ocean Rossby waves south of the equator, and anomalous cross-equatorial ocean heat transports contribute to the heat content anomalies in the Indian Ocean and thus to the ocean memory and consequent SST anomalies, which are an essential part of the TBO.

1. Introduction

The tropospheric biennial oscillation (TBO) has been defined as the tendency for a relatively strong monsoon to be followed by a relatively weak one, and vice versa, with the transitions occurring in the season prior to the monsoon involving coupled land–atmosphere–ocean processes over a large area of the Indo-Pacific region (Meehl 1994, 1997; Meehl and Arblaster 2001; 2002a,b). Thus, the system tends to flip-flop back and forth from year to year. The more of these interannual flip-flops or transitions, the more biennial the system.

An important part of any biennial mechanism is anomalous heat storage in the ocean and the associated SST anomalies that can occur in certain regions. Thus, the ocean retains the ''memory'' of ocean–atmosphere interaction over the course of a year to affect the atmosphere the following year (e.g., Brier 1978; Nicholls 1978; Chang and Li 2000; Li et al. 2001a; Meehl 1987, 1993). Several studies have suggested that coupled ocean dynamics plays a role in the formation and maintenance of these heat content and SST anomalies associated with the TBO (Meehl 1993; Clarke et al. 1998; Webster et al. 1999, 2003, manuscript submitted to *Quart. J. Roy. Meteor. Soc.*, hereafter W2003; Saji et al. 1999; Meehl and Arblaster 2002a; Loschnigg et al. 2003). Several of these papers (Webster et al. 1999; W2003; Saji et al. 1999) and others (Iizuka et al. 2000; Ashok et al. 2001; Vinayachandran et al. 2002; Saji and Yamagata 2003) have described the existence of a dipole or zonal SST mode in the tropical Indian Ocean that plays a role in monsoon variability in the region. Meehl and Arblaster (2002a) pointed out that

* Current affiliation: International Pacific Research Center, University of Hawaii at Manoa, Honolulu, Hawaii.

+ The National Center for Atmospheric Research is sponsored by the National Science Foundation.

Corresponding author address: Dr. Gerald A. Meehl, NCAR, P.O. Box 3000, Boulder, CO 80307-3000.
E-mail: meehl@ncar.ucar.edu

this Indian Ocean dipole or zonal mode is an integral part of coupled processes involved with the TBO. Meehl (1993) also noted significant upper-ocean heat content anomalies in regions of the tropical Pacific that contribute to the memory of the system and, thus, the TBO.

The purpose of this paper, then, is to analyze observations to elucidate the role of coupled ocean dynamical processes in the TBO regarding the formation and maintenance of heat content and SST anomalies in the tropical Indian and Pacific Oceans. Observed upper-ocean temperature data from several sources will be analyzed and related to composite TBO evolution.

In section 2 we will review the observational data used in this study, and in section 3 we will show composite TBO evolution in the atmosphere and sea surface. Then, in section 4 upper-ocean data from several sources will be formulated in similar composites to document the important role of coupled ocean dynamics in the TBO. In section 5 we will provide a synthesis of the atmospheric and ocean data to show the nature of the coupled ocean–atmosphere phenomena involved with the TBO. Section 6 will follow with conclusions.

2. Data

We use 21 years of observed data for the period January 1979–October 1999 including gridded Climate Prediction Center Merged Analysis of Precipitation (CMAP) precipitation data [Xie and Arkin (1996); the same time period was used in the companion studies of Meehl and Arblaster (2001, 2002a)] and 500-hPa heights and surface winds and temperatures from the National Centers for Environmental Prediction–National Center for Atmospheric Research (NCEP–NCAR) reanalysis data (Kalnay et al. 1996; Trenberth et al. 2001) for those same years. Therefore, there are 21 Indian monsoon years (1979–99), and 20 Australian monsoon years (1979–98), where December determines the year of the Australian monsoon from December–January–February (DJF; e.g., the Australian monsoon of 1980 would consist of December 1980, January 1981, and February 1981). All data are on a T42 grid. One source of upper-ocean monthly mean ocean temperature data from the equatorial Pacific for 1980–2000 is the NCEP reanalysis using an ocean data assimilation system (Ji et al. 1994, 1995). Upper-ocean dynamic height data for two selected locations in the Indian Ocean (0.51°S, 67.64°E; 6.76°S, 105.17°E) are from the Commonwealth Scientific and Industrial Research Organisation expendable bathythermograph (CSIRO XBT) network, which has been an operational Australian contribution to the Global Ocean Observing System (GOOS), jointly supported by the Bureau of Meteorology and CSIRO in Australia (Meyers and Pigot 1999; see http://www.marine.csiro.au/pigot/REPORT/). The time period that the data have in common for these two points is from late 1986 to mid 1999, with 1989 missing. Another source of upper-ocean reanalysis data for the Indian and Pacific Oceans is the University of Maryland Simple Ocean Data Assimilation (SODA; Carton et al. 2000a,b). Data are available from 1950–99 and 1979–99 are analyzed here to be consistent with the period analyzed from the precipitation data.

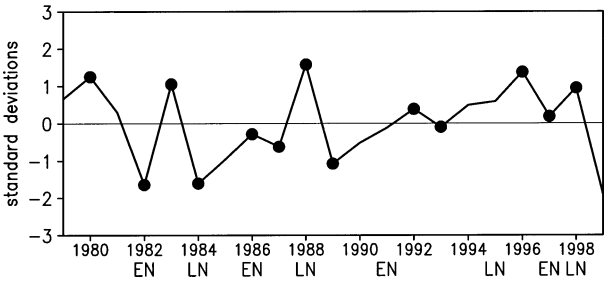

FIG. 1. (a) Time series of area-averaged Indian monsoon rainfall, JJAS, 1979–99, 5°–40°N, 60°–100°E; solid dots indicate TBO years when monsoon rainfall was relatively greater or less than preceding and following years, and El Niño (EN) and La Niña (LN) onset years are as indicated.

3. Composite TBO evolution

The time series of area-averaged precipitation for the Indian monsoon [June–July–August–September (JJAS), 1979–99, 5°–40°N, 60°–100°E] used in previous TBO analyses (Meehl and Arblaster 2001, 2002a) is shown in Fig. 1. Solid dots indicate monsoon rainfall relatively greater (or less) than the preceding and following years. That is, if P_i is the value of area-averaged monsoon season precipitation for a given year, i, then a relatively strong monsoon is defined as

$$P_{i-1} < P_i > P_{i+1}$$

and a relatively weak monsoon is defined as

$$P_{i-1} > P_i < P_{i+1}.$$

For the Indian monsoon, 13 out of 21 years are ''biennial'' defined in that way. El Niño and La Niña onset years correspond to some of those TBO years, but not all, as was first noted by Meehl (1987). For the composites in this paper, there are seven relatively strong monsoon years from Fig. 1 (1980, 1983, 1986, 1988, 1992, 1996, 1998), and six relatively weak (1982, 1984, 1987, 1989, 1993, 1997). El Niño (1982, 1986, 1991, 1997) and La Niña (1984, 1988, 1995, 1998) onset years are defined by Meehl and Arblaster (2002a) as the initiation of a five-month running mean area-averaged SST anomaly in the eastern tropical Pacific Niño-3 area (5°N–5°S, 150°–90°W) of at least ±0.5°C for two consecutive seasons after the March–April–May (MAM) transition season over the following 1-yr period. Of the TBO years in Fig. 1, 1982, 1986, and 1997 are El Niño onset years, and 1984, 1988, and 1998 are La Niña onset years for a total of six TBO years out of eight possible ENSO onset years. Thus, there are four remaining rel-

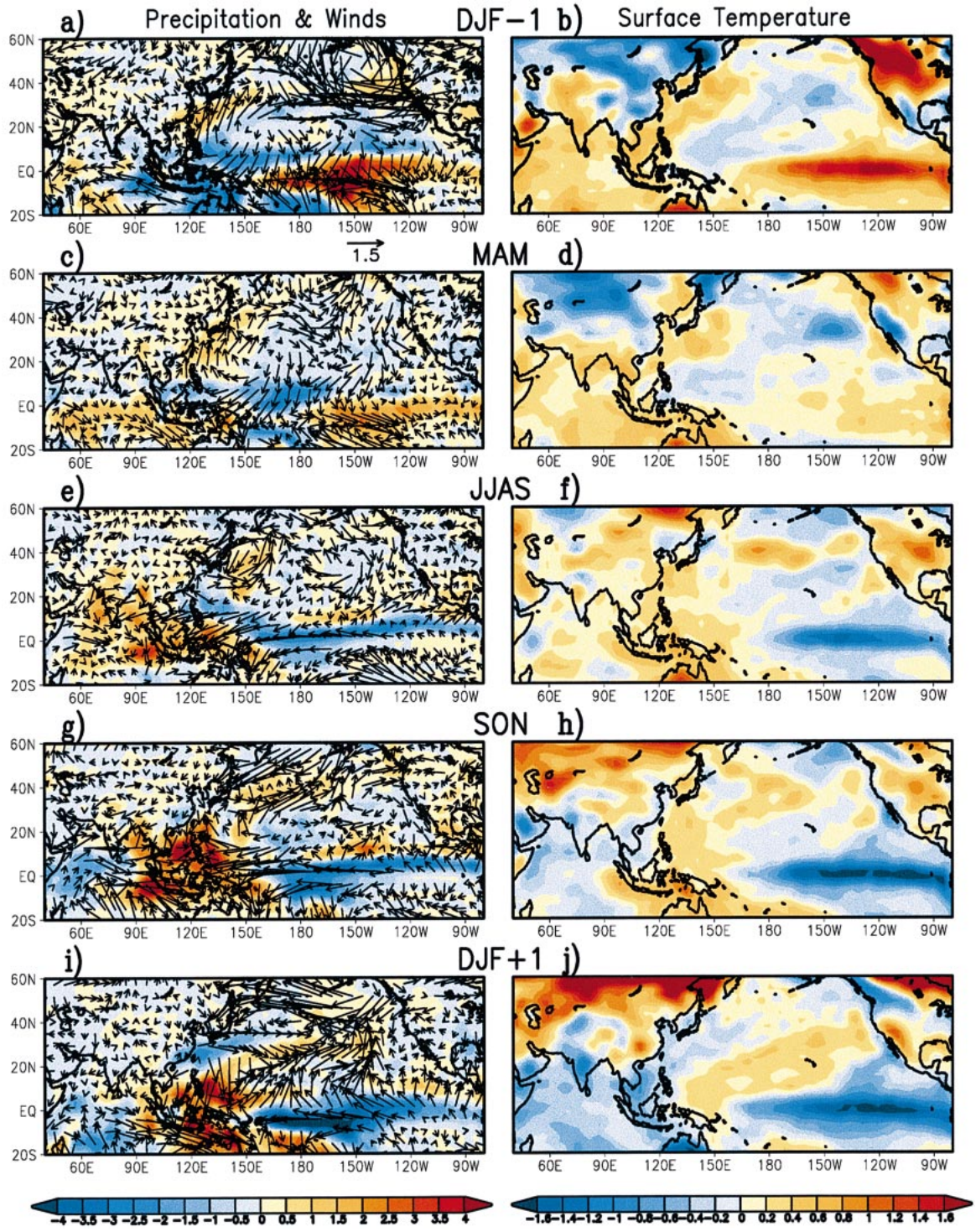

FIG. 2. Positive minus negative TBO Indian monsoon composites (years denoted by solid dots in Fig. 10c; seven relatively strong or positive TBO years, six relatively weak or negative TBO years) for seasons lagging and leading the Indian monsoon. (a) Precipitation and winds for DJF prior to the Indian monsoon; (b) surface temperature for DJF prior to the Indian monsoon; (c) precipitation and winds for MAM prior to the Indian monsoon; (d) surface temperature for MAM prior to the Indian monsoon; (e) precipitation and winds for JJAS Indian monsoon season; (f) surface temperature for JJAS Indian monsoon season; (g) precipitation and winds for SON after the Indian monsoon; (h) surface temperature for SON after the Indian monsoon; (i) precipitation and winds for DJF after the Indian monsoon; (j) surface temperature for DJF after the Indian monsoon. Units are m s^{-1}, mm day^{-1}, and °C for surface wind, precipitation, and surface temperature, respectively. Scaling vector above (c) is 1.5 m s^{-1}.

atively strong monsoon years (1980, 1983, 1992, 1996) and three relatively weak (1987, 1989, 1993).

As noted by Meehl (1987), defining relatively strong and weak monsoons in this way removes low-frequency variability. However, it also can result in, for example, a strong monsoon compared to previous and following years lying below the long-term mean (e.g., 1986). It is also worth noting that connections between the tropical Pacific and the Indian monsoon vary with time (e.g., Kumar et al. 1999). For the time period considered here after the late 1970s, this connection has been weak compared to other periods. Thus, the implication for this analysis is that the linkage for this time period may actually be stronger in different eras. Additionally, the strong monsoon years include negative (cold) Indian Ocean dipole (IOD) years such as 1992 and 1996, and weak years contain positive (warm) IOD years (e.g., 1982, 1997) as noted by Saji et al. (1999). These strong interannual events contribute to the composites and help make the case that TBO processes encompass IOD variability in the Indian Ocean.

The spectra of this time series (shown by Meehl and Arblaster 2002a, their Fig. 2) show a maximum in the TBO period of 2.6 yr with little ENSO peak for this time period, though the relative power of ENSO and TBO varies over time (e.g., Webster et al. 1998; Torrence and Webster 1999). Comparable spectra for Australian monsoon rainfall time series show TBO and ENSO peaks around 2.5 and 6 yr, respectively (Meehl and Arblaster 2002a, their Fig. 2). It has been shown that transitions of the Indian monsoon tend to ''set'' the system for the subsequent Australian monsoon (Meehl 1987, 1997; Shukla and Paolino 1983; Kiladis and van Loon 1988; Webster and Yang 1992). Therefore, in this paper we will form strong minus weak composites to analyze TBO coupled interactions for the entire cycle from the Indian monsoon to the Australian monsoon.

Meehl and Arblaster (2002a,b) quantified the contributions of three elements of the Indo-Pacific region to the TBO, with tropical Pacific SSTs being a major contributor. Thus, without the tropical Pacific, processes in the Indian region can still produce the TBO as in Li et al (2001a) and Chang and Li (2000). But without the contribution from the Pacific, the TBO amplitude is weaker. TBO thus encompasses El Niño. Chang and Li (2000) argue that the TBO can arise solely in the Indian region without the Pacific, which was confirmed in the modeling study of Meehl and Arblaster (2002b). However, inclusion of the Pacific influence raises the TBO amplitude. Torrence and Webster (1999) also show that in periods of large ENSO amplitude represented by Niño-3 SSTs, the TBO in Niño-3 SSTs is strong as well.

The singular value decomposition (SVD) regressions in Meehl and Arblaster (2002a) provide information concerning the processes associated with TBO transitions. They break down the TBO into the components related to the transition conditions and provide quantification of those separate transition conditions vital to producing the TBO. Here we return to a more holistic picture of TBO evolution through the use of composites that inherently combine the separate transition conditions (500-hPa height–Asian land temperature anomalies, tropical Indian and Pacific SST anomalies) documented by Meehl and Arblaster (2001, 2002a,b).

For the TBO years defined in Fig. 1, we composite precipitation, surface temperature, and surface winds for the relatively strong (positive) and relatively weak (negative) monsoon years, and compute positive minus negative TBO composites in Fig. 2 to show the evolution from the DJF prior to the Indian monsoon (DJF $-$ 1) to the DJF after (DJF + 1). Computing a standard *t* test and showing only significant differences would reduce the amount of information in Fig. 1 and elsewhere in this paper. Therefore, we choose to show all the differences here (in consideration of the relatively short sample size) and interpret the physical significance of the results (e.g., Nicholls 2001).

For the DJF season prior to the relatively strong Indian monsoon (DJF $-$ 1 in Figs. 2a,b), there is a weak Australian monsoon with negative precipitation anomalies of around 2–3 mm day^{-1} (around 20%) over much of the Australian monsoon region. There are anomalously warm SSTs greater than 1.5°C in the equatorial central and eastern Pacific with westerly wind anomalies of about 1.5 m s^{-1} in the central equatorial Pacific consistent with the enhanced precipitation there. However, there are easterly anomaly surface winds of roughly 0.8 m s^{-1} in the far western equatorial Pacific, and somewhat stronger easterly anomaly winds across the equatorial Indian Ocean. These are dynamically consistent with the negative rainfall anomalies and anomalous sinking air there (e.g., Clarke 1994). They are also associated with enhanced precipitation over the central tropical Pacific and western Indian Oceans, respectively, and somewhat warmer SSTs in the equatorial western Indian Ocean (about $+0.5$°C) compared to the east (less than $+0.2$°C). By MAM (Figs. 2c,d) there is a band of suppressed precipitation across about 10°N from the Indian to Pacific (values of about -0.5 to -1.0 mm day^{-1}). There also are small-amplitude westerly wind anomalies in the far western equatorial Indian Ocean, warm SSTs of about $+0.2$ to $+0.4$°C in the Indian Ocean, and small positive SST anomalies in the eastern equatorial Pacific along with continued easterly component wind anomalies of about 0.7 m s^{-1} from 120° to about 160°E in the western equatorial Pacific. The wind anomalies in the equatorial far-western Pacific are part of the anomalous west Pacific anticyclone (WPA) as noted by Lau and Wu (2001) and Kim and Lau (2001).

In JJAS (Figs. 2e,f) there are positive precipitation anomalies of around $+1.0$ to $+2.0$ mm day^{-1} (roughly 20%–25%) over much of south and southeast Asia and the Indian Ocean. There are also negative precipitation (-1.0 mm day^{-1}) and SST (-1.0°C) anomalies over the central and eastern tropical Pacific and an east–west precipitation anomaly pattern between Australasia (pos-

itive anomalies) and the tropical western Pacific (negative anomalies). Additionally, there are westerly wind anomalies of about 1.0 m s^{-1} across the western equatorial Indian Ocean associated with a cooling of SSTs of a couple of tenths of a degree in the far western Indian Ocean, and the appearance of a negative dipole (anomalous gradient) of SSTs across the equatorial Indian Ocean. This pattern, with anomalously cold SSTs in the west, warm in the east, is the opposite phase of the positive dipole described in Webster et al. (1999) that had anomalously warm SSTs in the west, and cold in the east. In the canonical TBO evolution, such a positive dipole would occur in association with a relatively weak south Asian monsoon a year after the appearance of the negative dipole and strong south Asian monsoon shown here.

Figure 2e also shows easterly anomaly winds of about 0.5 m s^{-1} in the central Indian Ocean near 10°S, 80°E. Easterly anomaly surface winds extend nearly all the way across the equatorial Pacific with largest values of about 1.0 m s^{-1}.

The September–October–November (SON) pattern in Figs. 2g,h resembles the Indian Ocean–related SVD regressions in Meehl and Arblaster (2002a, their Figs. 15g,h) with a strong convective maximum over Southeast Asia and values greater than +2.0 mm day^{-1}, warm SSTs of about half a degree in the vicinity of Indonesia and Australia in the path of the seasonal movement of the convective maximum, westerly anomaly winds greater than 1.5 m s^{-1} in the Indian Ocean, and a negative SST dipole (anomalous SST gradient) across the equatorial Indian Ocean with negative SST anomalies of about −0.5°C in the west and positive anomalies of about +0.8°C in the east. Easterly wind anomalies with maximum values of about 1.3 m s^{-1} and cool SSTs in excess of −1.5°C persist in the central and eastern equatorial Pacific.

The enhanced convective maximum that started with the Indian monsoon in JJAS and stayed that way in SON over Southeast Asia remains strong in the following DJF + 1 in Figs. 2i,j. There is a strong Australian monsoon with positive precipitation anomalies of greater than +2.0 mm day^{-1} over most of the monsoon domain of Indonesia, Papua New Guinea, and northern Australia. There is the appearance of westerly anomaly surface winds of about 0.5 m s^{-1} associated with the enhanced precipitation in the western equatorial Pacific, and westerly anomaly winds of around 1.0 m s^{-1} in the eastern Indian Ocean south of the equator associated with strong inflow into the Australian monsoon. The negative dipole of SST anomalies in the Indian Ocean evident in SON has now evolved to uniform negative anomalies of around −0.4° to −0.6°C covering the entire Indian Ocean in DJF + 1. The westerly surface wind anomalies at the equator in the Indian Ocean have weakened by a factor of about 3 (compared to SON) to less than 0.5 m s^{-1}.

To examine the effect of ENSO onset years on the TBO composites here, the non-ENSO year composites (noted earlier) for the TBO evolution are shown in Fig. 3. Virtually every feature noted above to occur in all TBO years in Fig. 2 appears in Fig. 3 but with reduced magnitude. This corroborates the earlier results of Meehl (1987) who showed that there are years other than ENSO onset years that have similar signatures of anomalous precipitation and SST patterns to ENSO onset years. The former have lower amplitudes but still contribute to the TBO. Here we see a similar result confirmed for SSTs but with the addition of precipitation and surface wind data. This strengthens the idea that the TBO encompasses most ENSO El Niño and La Niña years [with their biennial tendency (e.g., van Loon 1986; Kiladis and van Loon 1988; Kiladis and Diaz 1989); though protracted El Niño conditions can occur that weaken this aspect of the biennial signal in ENSO (e.g., Allan and D'Arrigo 1999; Li et al. 2001a)], as well as additional years with similar but lower-amplitude signals that contribute to the TBO.

The composite evolution of strong minus weak monsoon years in Fig. 2 for all TBO years and Fig. 3 for non-ENSO onset years resembles many aspects of the evolution described from SVD analyses by Meehl and Arblaster (2002a). However, there are more identifiable features here from the Indian Ocean and Pacific SST relationship than the midlatitude 500-hPa circulation-related components over Asia. This provides additional confirmation to the GCM sensitivity experiments of Meehl and Arblaster (2002b) that forcing of 500-hPa circulation from convective heating anomalies in the Tropics in seasons prior to the Indian monsoon is a secondary factor, though more important in some years than others (e.g., Meehl and Arblaster 2002a, their Fig. 10). The meridional temperature gradient effects, induced by land–sea temperature contrasts among other things, contribute to more rain falling over some south Asian land areas and less over the Indian Ocean, and appear linked to a more hemispheric pattern of enhanced ITCZ-like rainfall extending from India to the Pacific. Additionally, Li et al. (2001b) have shown that regional forcing from Indian Ocean SST anomalies with effects on monsoon rainfall is more dominant in the TBO than SST forcing from either the tropical eastern Pacific or from meridional temperature gradients over Asia. Clark et al. (2000) have also shown strong TBO associations between Indian Ocean SSTs and monsoon rainfall in recent decades.

The large-scale east–west circulation linking the Indian and Pacific sectors has always been a central element of the TBO mechanism being studied here (Meehl 1987, 1997). Documentation of this circulation is difficult, but it was shown in a GCM sensitivity experiment that the connection of SST anomalies from the tropical Pacific for a TBO transition mechanism involved the Walker circulation (Meehl and Arblaster 2002b). The latter was documented as anomalies of vertical velocity (omega) in the model. Here we composite vertical ve-

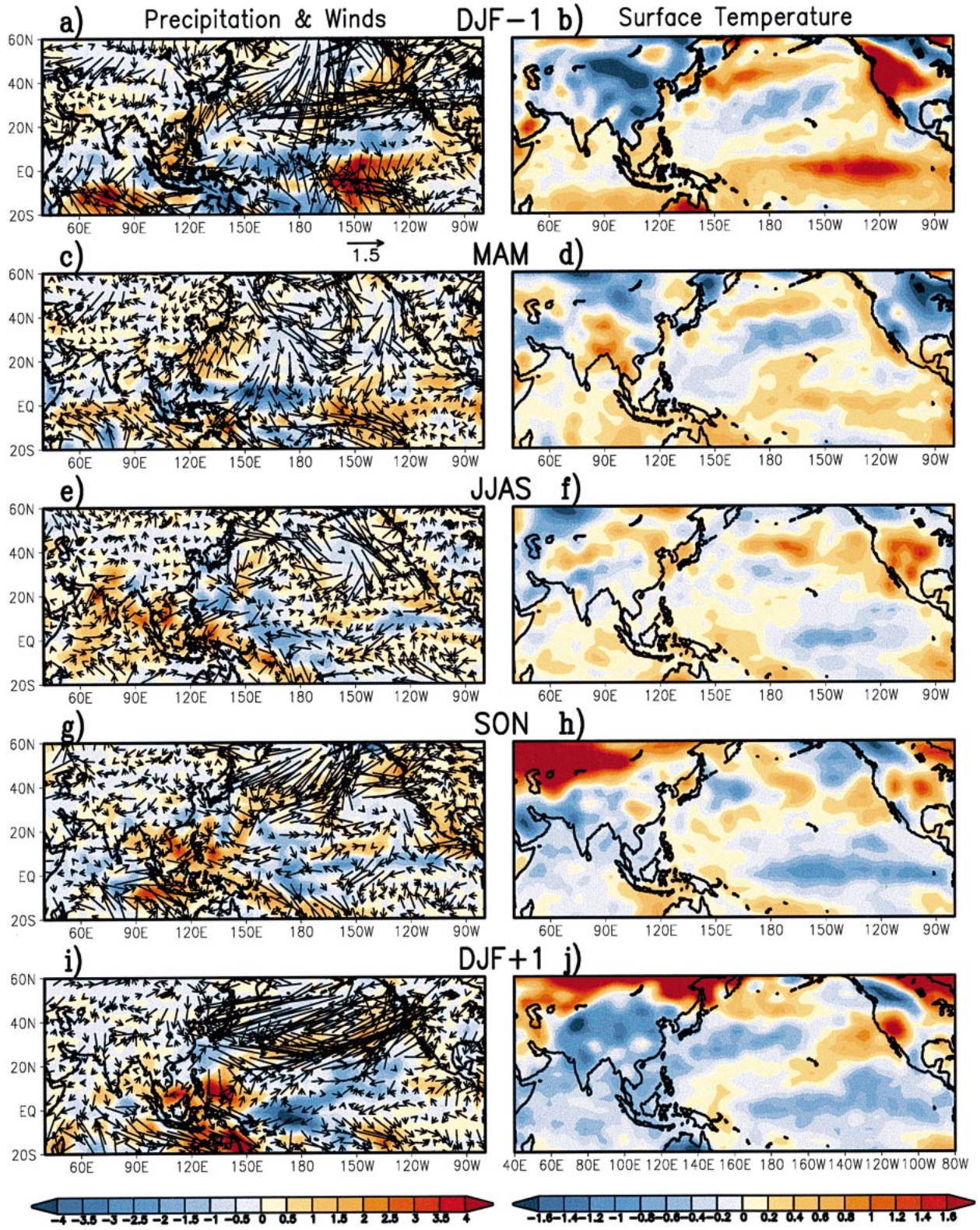

FIG. 3. Same as Fig. 2 except for composites excluding El Niño and La Niña onset years (four relatively strong or positive TBO years, and three relatively weak or negative TBO years).

locity (omega) from the reanalyses averaged over 5°N–5°S to show how the large-scale east–west circulations link various parts of the Indo-Pacific region in the TBO. Figure 4 shows composite vertical velocity for the time evolution in Figs. 2 and 3 for all TBO strong minus weak years (Figs. 4a,c,e,g,i) and non-ENSO TBO years (Figs. 4b,d,f,h,j). For this quantity, negative differences indicate anomalous upward vertical velocity.

In DJF − 1, the weak Australian monsoon noted in Fig. 2a is indicated by positive midtroposphere anomaly values of omega (indicative of anomalous subsidence) of greater than 1.0 hPa $s^{-1} \times 10^{-4}$ in the neighborhood of 130°E. Warm SSTs and anomalous positive precipitation anomalies in the tropical Pacific are represented by negative midtroposphere omega values (anomalous ascent) of greater than −1.2 hPa $s^{-1} \times 10^{-4}$ east of the date line. This pair of opposite-sign omega anomalies indicates an anomalously weakened eastern Walker cell [defined as the Walker circulation linking Australasia and the eastern Pacific as shown in Meehl and Arblaster (2002a)]. The climatological eastern and western Walker cells at this time of year are characterized by strong ascent associated with Australian monsoon rainfall, and subsidence over the western Indian and eastern Pacific Oceans. Meanwhile, there are anomalous negative omega values west of 90°E (anomalous ascent) associated with the positive precipitation anomalies there in Fig. 2a. This part of the large-scale east–west atmospheric circulation will be referred to as the western Walker cell (as in Meehl and Arblaster 2002a), and it is anomalously weak at this stage of the TBO as well.

For MAM in Fig. 4c, there is a weakening of the negative omega anomalies by about a factor of 2 compared to DJF − 1 in Fig. 4a associated with the start of the transition of SST anomalies in the eastern Pacific from positive to negative in Fig. 2c. There is a similar weakening of the positive omega anomalies in the western Pacific. However, the Walker circulation is still anomalously weak for both western and eastern Walker cells as in Fig. 4a.

By JJAS in Fig. 4e, the strong south Asian monsoon and anomalously cold SSTs in the eastern Pacific (Fig. 2e) are associated with negative omega anomalies (anomalous ascent) from 60° to 150°E with maxima of over −1.4 hPa $s^{-1} \times 10^{-4}$, and large positive anomalies (anomalous subsidence) east of the date line with maxima greater than +1.5 hPa $s^{-1} \times 10^{-4}$. There are also positive omega anomalies (anomalous subsidence) with maxima of about +1.0 hPa $s^{-1} \times 10^{-4}$ west of 60°E. Therefore, the sense of the entire anomalous east–west atmospheric circulation in these regions has reversed from MAM to JJAS. In JJAS there are now anomalously strong western (positive west of 60°E, negative 60°–155°E) and eastern (negative 60°–155°E, positive 155°E–100°W) Walker cells signified by strong anomalous ascent over the south Asian monsoon region, and anomalous subsidence over the western Indian and eastern Pacific Ocean areas.

With the strong convective maximum traversing Southeast Asia in SON, continued negative SST anomalies and suppressed convection in the eastern Pacific, and the growth of negative SST and precipitation anomalies in the western Indian Ocean in SON (Figs. 2g,h), there are associated anomalously strong western and eastern Walker cells as indicated by the omega anomaly patterns in Fig. 4g that are similar to Fig. 4e. With the establishment of the SST dipole (anomalous SST gradient) across the equatorial Indian Ocean, the positive omega anomalies have moved east and extend west from 90°E in Fig. 4g. Negative omega anomalies indicating more intense vertical motion associated with the strong convective maximum with peak midtroposphere values greater than −1.5 hPa $s^{-1} \times 10^{-4}$ occur from about 90°E to the date line, and large-amplitude positive omega anomalies remain east of the date line. The sense of the anomalous large-scale east–west atmospheric circulation remains the same as in JJAS, with anomalously strong western and eastern Walker cells.

By DJF + 1 in Fig. 4i, the strong Australian monsoon in Fig. 2i is associated with peak anomalous negative omega values (anomalous ascent) greater than −1.5 hPa $s^{-1} \times 10^{-4}$ near 125°E, and positive omega anomalies east of the date line and west of about 90°E (anomalous subsidence), maintaining the sense of the anomalously strong eastern and western Walker cells from the previous two seasons in Figs. 4e,g.

The companion omega anomaly plots for the non-ENSO onset TBO years in Figs. 4b,d,f,h,j have the same patterns as for the all TBO years composites except for magnitudes reduced by about a factor of 2. Therefore, for omega anomalies as well as for the precipitation, surface temperature, and surface wind composites in Figs. 2 and 3, similar but lower-amplitude anomalies exist in a greater set of years than just ENSO El Niño and La Niña events. This confirms the previous assertion that the TBO encompasses most ENSO years, but includes other years as well with comparable but lower-amplitude anomalies. This then contributes to the introduction of a biennial component into spectra of monsoon rainfall time series, the TBO, as noted by Meehl and Arblaster (2002a).

4. Upper-ocean data analyses

a. Pacific Ocean temperature

It is evident that the transition of SSTs in the Pacific associated with the TBO is linked directly to Australian monsoon precipitation anomalies and associated surface wind anomalies in the far western equatorial Pacific through the eastern Walker cell. Meehl and Arblaster (2002a) postulated that the weak Australian monsoon and easterly surface wind anomalies in the far western equatorial Pacific (Figs. 2a,b) set off upwelling Kelvin waves and a subsequent shallowing of the thermocline in the eastern equatorial Pacific. This contributes to the

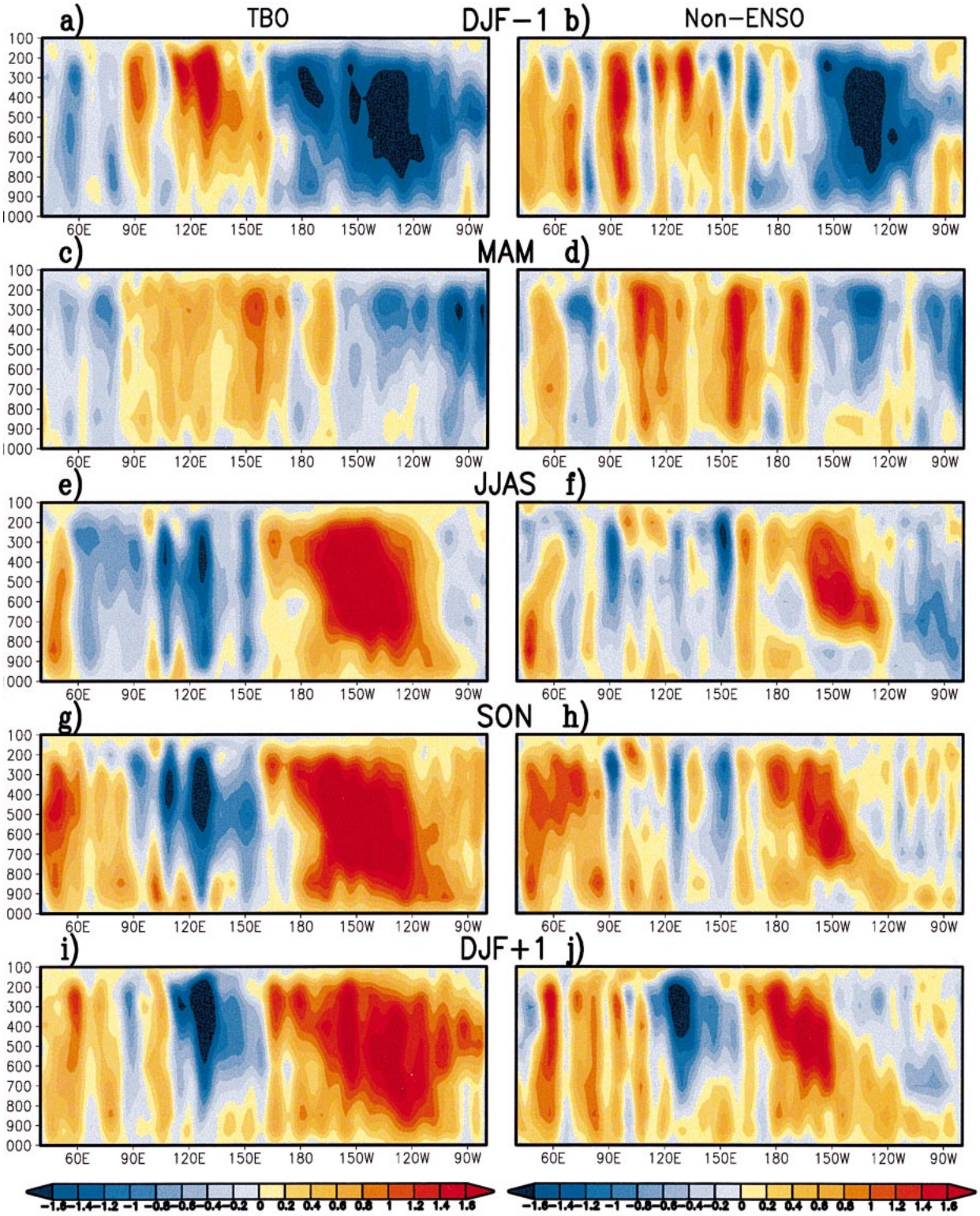

FIG. 4. Same as Fig. 2 except for composites of omega (vertical velocity, hPa $s^{-1} \times 10^{-4}$), averaged over 5°N–5°S.

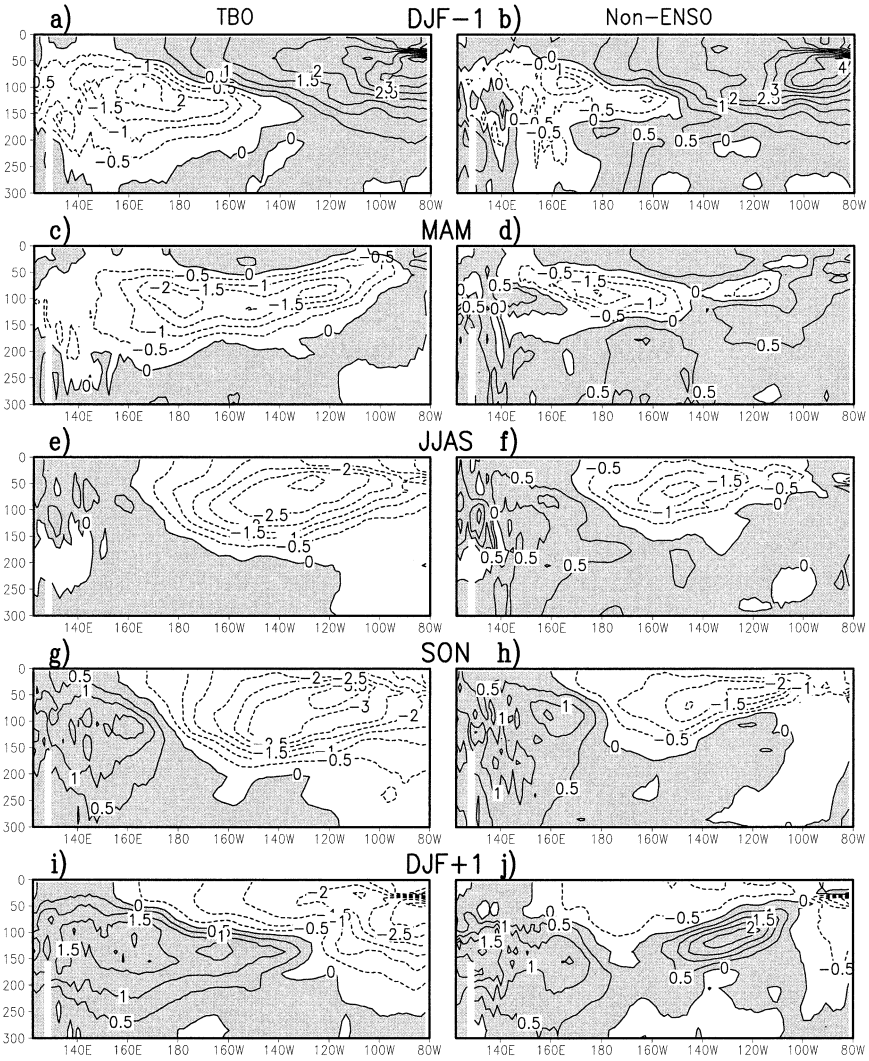

FIG. 5. Positive minus negative composites for upper-ocean temperatures in the equatorial Pacific (°C), positive minus negative TBO Indian monsoon years (denoted by solid dots in Fig. 10c; seven relatively strong or positive TBO years, six relatively weak or negative TBO years) (left) for all TBO years and (right) non-ENSO onset TBO years (the same sets of years used to formulate Figs. 2 and 3, respectively) for seasons lagging and leading the Indian monsoon. (a) Equatorial upper-ocean temperatures for all TBO years and (b) non-ENSO onset TBO years for DJF prior to the Indian monsoon; (c) all TBO years and (d) non-ENSO onset TBO years for MAM prior to the Indian monsoon; (e) all TBO years and (f) non-ENSO onset TBO years for JJAS Indian monsoon season; (g) all TBO years and (h) non-ENSO onset TBO years for SON after the Indian monsoon; (i) all TBO years and (j) non-ENSO onset TBO years for DJF after the Indian monsoon. Positive anomalies are shaded; contour interval is 0.5°C.

transition from warm to cold SST anomalies in the Pacific farther east starting in MAM and continuing to JJAS. In Fig. 5, composites of upper-ocean temperatures from the NCEP ocean reanalyses in the equatorial Pacific for positive minus negative TBO Indian monsoon years are plotted for all TBO years and non-ENSO onset TBO years (the same sets of years used to formulate Figs. 2–4). For both composites in DJF − 1 (Figs. 5a,b) anomalously cool temperatures in the western equatorial Pacific extend below 200 m with largest-amplitude anomalies greater than −2°C near 100 m in Fig. 5a, and near −1°C in Fig. 5b. There are anomalously warm temperatures (greater than +1°C) in the central and eastern Pacific down to about 100–200-m depth, with maximum anomalies near +4°C in the far eastern equatorial Pacific around 75 m. Associated with the easterly anomaly surface winds in the far western equatorial Pacific in DJF − 1 (Fig. 2a), by MAM the collection of upwelling Kelvin waves are manifested as negative temperature anomalies of −1° to −2°C across the Pacific at the level of the thermocline ranging from near 125-m depth near the date line to about 75 m near 120°W

(Figs. 5c,d). At this time easterly anomaly winds in MAM extend farther east to about the date line (Fig. 2c). Easterly anomaly surface currents that started in DJF − 1 in the far western equatorial Pacific in association with the easterly anomaly surface winds stretch across the equatorial Pacific in MAM with maximum values of about −15 cm s^{-1} (not shown).

While these changes are taking place, the positive surface temperature anomalies in the central and eastern equatorial Pacific in DJF − 1 have weakened considerably by MAM (as was noted in Figs. 2b,d). By JJAS there are negative temperature anomalies established from near the date line to the eastern Pacific (Fig. 2f), extending through the depth of the upper ocean to below 110 m for all TBO years as well as the non-ENSO years (Figs. 5e,f) with values of around −2° to −3°C. Easterly anomaly surface currents with values around −17 cm s^{-1} remain established across the equatorial Pacific in JJAS (not shown). Positive temperature anomalies of about +0.5°C are now appearing around 50 m in the far western Pacific for both as well (Figs. 5e,f). The strong convective maximum associated with the relatively strong south Asian monsoon in JJAS (Fig. 2e) continues with the seasonal cycle to SON. At this time there are strong easterly anomaly surface winds (Fig. 2g) and surface currents greater than −15 cm s^{-1} (not shown) across the equatorial Pacific that contribute to building warm temperature anomalies greater than +1°C in the western Pacific through the depth of the upper ocean to below 200 m (Figs. 5g,h). As the strong convection proceeds to the Australian monsoon and western Pacific region in DJF + 1 (Fig. 2i), westerly anomaly winds associated with the positive precipitation anomalies in the western equatorial Pacific set off downwelling Kelvin waves. These appear as positive temperature anomalies greater than +1.5°C at the thermocline level farther east (Figs. 5i,j) to complete the TBO evolution. The magnitudes of these anomalies are near or exceed one standard deviation (not shown). Further discussion of anomaly magnitude compared to variability will accompany Figs. 8 and 9.

This ocean dynamical response was suggested by analysis of ocean station data for limited regions of the western and eastern Pacific by Meehl (1993). As in Fig. 5, the largest upper-ocean temperature response in the western Pacific was shown by that study to be at the depth of the thermocline and was present for all TBO years and non-ENSO TBO years as well [also shown for a limited region north of New Guinea by Yasunari (1990)]. Though no surface wind data was available for the Meehl (1993) analyses and only annual means of limited upper-ocean temperature data for certain periods in the TBO evolution were used, the changes in upper-ocean temperature structure shown in that study are consistent with the composite differences in Figs. 2 and 5. However, the seasonal data from the Pacific Ocean reanalyses provide much better time resolution and show that the wind forcing is consistent with the ocean dynamical response. It also shows that similar coupled processes occur in years other than ENSO, as shown for ocean station data by Meehl (1993). The distinguishing characteristic is that ENSO events have larger-amplitude heat content anomalies (see also Meinen and McPhaden 2000).

b. Indian Ocean temperature

It has been suggested that ocean dynamics in the Indian Ocean are important for SST signals and coupled interactions involving the TBO and associated monsoon circulations there (Saji et al. 1999; Webster et al. 1999; W2003; Loschnigg and Webster 2000; Loschnigg et al. 2003). To examine this Indian Ocean dynamical connection in the present TBO context, we first analyze XBT data from a limited number of ship tracks for the Indian Ocean (Meyers and Pigot 1999). The wind evolution in Figs. 2 and 3 is consistent with Meehl (1993) for changes to upper-ocean temperatures. It is seen to better advantage for the seasonal evolution in composite normalized differences of dynamical height for two points: one near 0°, 67°E in the west-central Indian Ocean; and the other near 7°S, 105°E in the eastern Indian Ocean shown in Fig. 6. The dynamic height differences are oriented such that positive values are plotted below the zero line to indicate an anomalously deeper thermocline (i.e., a large positive normalized composite dynamic height difference indicates a thicker layer of warmer water, implying not only elevated sea level but a deeper thermocline and greater heat content). The relative anomalies between western and eastern Indian Ocean points are indicative of anomalous slope of the thermocline.

In January before a strong monsoon (top of Fig. 6), the all-TBO year normalized composite differences show an anomalous thermocline tilt upward to the east with negative dynamic height anomalies of about −0.7 standard deviations in the east. The non-ENSO onset years show the opposite anomalous thermocline orientation. However, by April both the all-TBO and non-ENSO TBO years show dynamic height differences that indicate an anomalous thermocline tilt downward to the east (an anomalously deeper thicker layer of water in the east), with values in the east exceeding one standard deviation. This is maintained through July and into October, consistent with the SST evolution described in Figs. 2 and 3. Thus, the ocean dynamical response to anomalous westerly winds in the western Indian Ocean is to deepen the thermocline in the east relative to the west. This result is expected theoretically at long timescales and has been previously documented for the Pacific (e.g., Kessler 1990). By January after the strong monsoon (bottom of Fig. 6), the sign of the dynamic height anomalies has changed to negative in the west in both composites, indicating a beginning of a transition to the opposite-sign composite anomalies the following year.

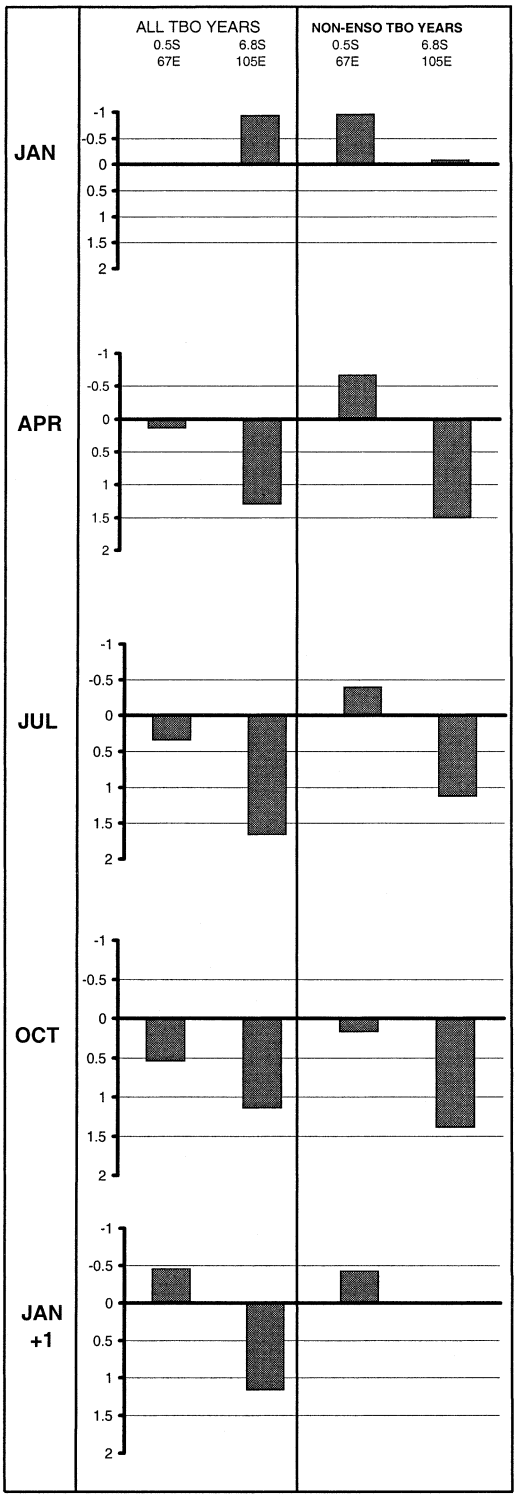

FIG. 6. Seasonal evolution, positive minus negative TBO Indian monsoon years, of composite normalized differences of dynamical height (Meyers and Pigot 1999) for two points in the Indian Ocean, one at 0.5°S, 67.6°E in the west-central Indian Ocean, and the other at 6.8°S, 105.2°E in the eastern Indian Ocean shown for the time period in common of available data from 1986 to 1999 (1989 missing), (left) for all TBO (years four strong or positive TBO years, three weak or negative TBO years) and (right) non-ENSO onset TBO years (two positive and two negative). The dynamic height differences are oriented such that positive values are below the zero line to indicate anomalous thermocline depth variations (e.g., a large positive normalized composite dynamic height difference indicates a thicker layer of warmer water, implying elevated sea level and a deeper thermocline with greater heat content). Thus, the relative anomalies between western and eastern Indian Ocean points are indicative of anomalous slope of the thermocline. Evolution from top to bottom of Jan prior to Indian monsoon, Apr prior to Indian monsoon, Jul of Indian monsoon season, Oct after Indian monsoon, and Jan after Indian monsoon.

An ocean reanalysis product that includes data from both the Indian and Pacific Oceans is the SODA dataset described earlier. A similar analysis with these data can provide a consistency check with the NCEP Pacific upper-ocean data and the XBT data from the Indian Ocean. First, to relate the thermocline depth with upper-ocean interannual variability, Fig. 7 shows the climatological seasonal mean equatorial sections of upper-ocean temperature, and Fig. 8 the seasonal interannual standard deviation for the period 1979–99. Clearly, temperature variability in all seasons is greatest at the level of the thermocline (i.e., depth of greatest vertical temperature gradient) in both the equatorial Indian and Pacific Oceans. This occurs at somewhat shallower levels in the Indian Ocean (around 100 m with maximum standard deviations of about 2°C in the eastern Indian Ocean) than in the western Pacific (around 140 m with maximum standard deviations of around 1°C west of the date line). However, as the thermocline slopes upward to the east in the Pacific, standard deviations also increase with maximum values of about 3°C east of 140°W, with shallowest thermocline depths of about 50 m near 90°W.

The features in Figs. 7 and 8 provide the context for the positive minus negative TBO composites in Fig. 9 (differences in the Pacific can also be compared to the NCEP data in Fig. 5). The all-TBO year composites are to the left of Fig. 9, and the non-ENSO onset year composite differences to the right. Both Indian and Pacific are plotted as in Figs. 7 and 8. The blank space between about 100° and 110°E is the island mass of Indonesia. First, for the Pacific, comparable evolution and magnitudes of anomalies to Fig. 5 are seen in Fig. 9. The shallowing of the thermocline is represented by negative anomalies working across the Pacific at the depth of the thermocline from DJF − 1 to MAM to JJAS. Maximum anomalies are about −2°C west of 150°W and greater than −3°C farther east, thus exceeding one standard deviation in those areas in Fig. 8. The thermocline in the western Pacific deepens as in Fig. 5, indicated by positive temperature anomalies greater than +1°C (exceeding one standard deviation in Fig. 8) near 140 m in SON and DJF + 1.

The XBT data in Fig. 6 indicated an anomalous tilt of the thermocline in the Indian Ocean with shoaling in the west and deepening in the east as the cold dipole

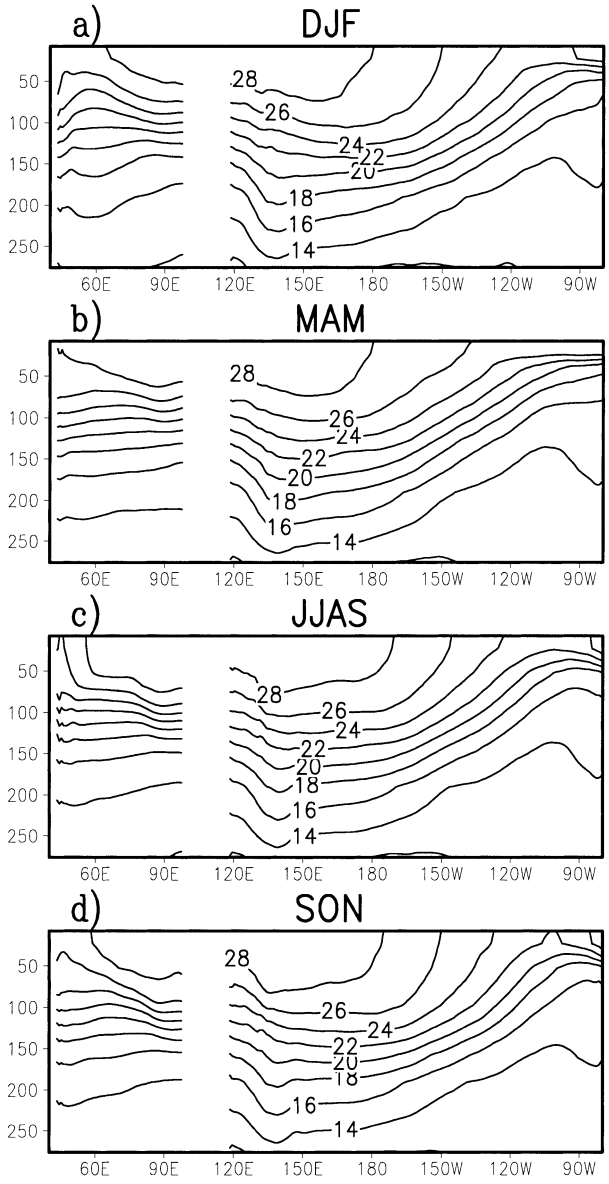

FIG. 7. Long-term mean climatology (1979–99) of upper-equatorial Indian and Pacific Ocean temperatures (°C; Carton et al. 2000a,b) for (a) DJF, (b) MAM, (c) JJAS, and (d) SON.

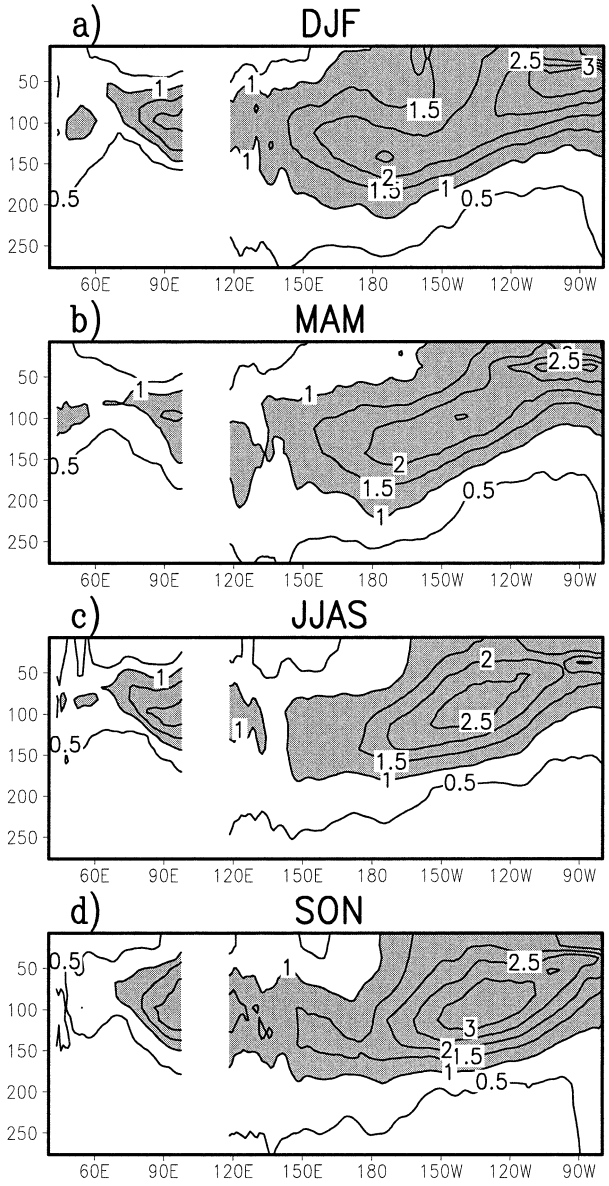

FIG. 8. Interannual standard deviations (°C) for upper-equatorial Indian and Pacific Ocean temperatures (Carton et al. 2000a,b) for (a) DJF, (b) MAM, (c) JJAS, and (d) SON.

(anomalous equatorial SST gradient, with cool water in the west and warm in the east) of SSTs develops from JJAS to SON. This is seen in the left parts of the panels in Fig. 9, where positive temperature anomalies at the depth of the thermocline near 100 m in DJF − 1 in the west propagate across the Indian Ocean basin near that depth in MAM so that by JJAS there are positive anomalies greater than +1.5°C in the eastern equatorial Indian Ocean, and small amplitude negative anomalies in the west. These temperature anomalies indicate an anomalous slope of the thermocline down to the east, consistent with the XBT results in Fig. 6. This subsurface dipole or temperature gradient in the Indian Ocean intensifies in SON with maximum positive temperature anomalies in the east greater than +2°C exceeding one standard deviation in that region in SON.

By DJF + 1 in Fig. 9, the surface temperature anomalies now are negative right across the equatorial Indian Ocean, with only a remnant of positive temperature anomalies in the east near 100 m. The transition from positive to negative SST anomalies in the far eastern tropical Indian Ocean is likely associated with anomalous surface heat flux forcing (Hendon 2003). As for all the other TBO composites presented so far, the non-ENSO composites at the right of Fig. 9 have very similar

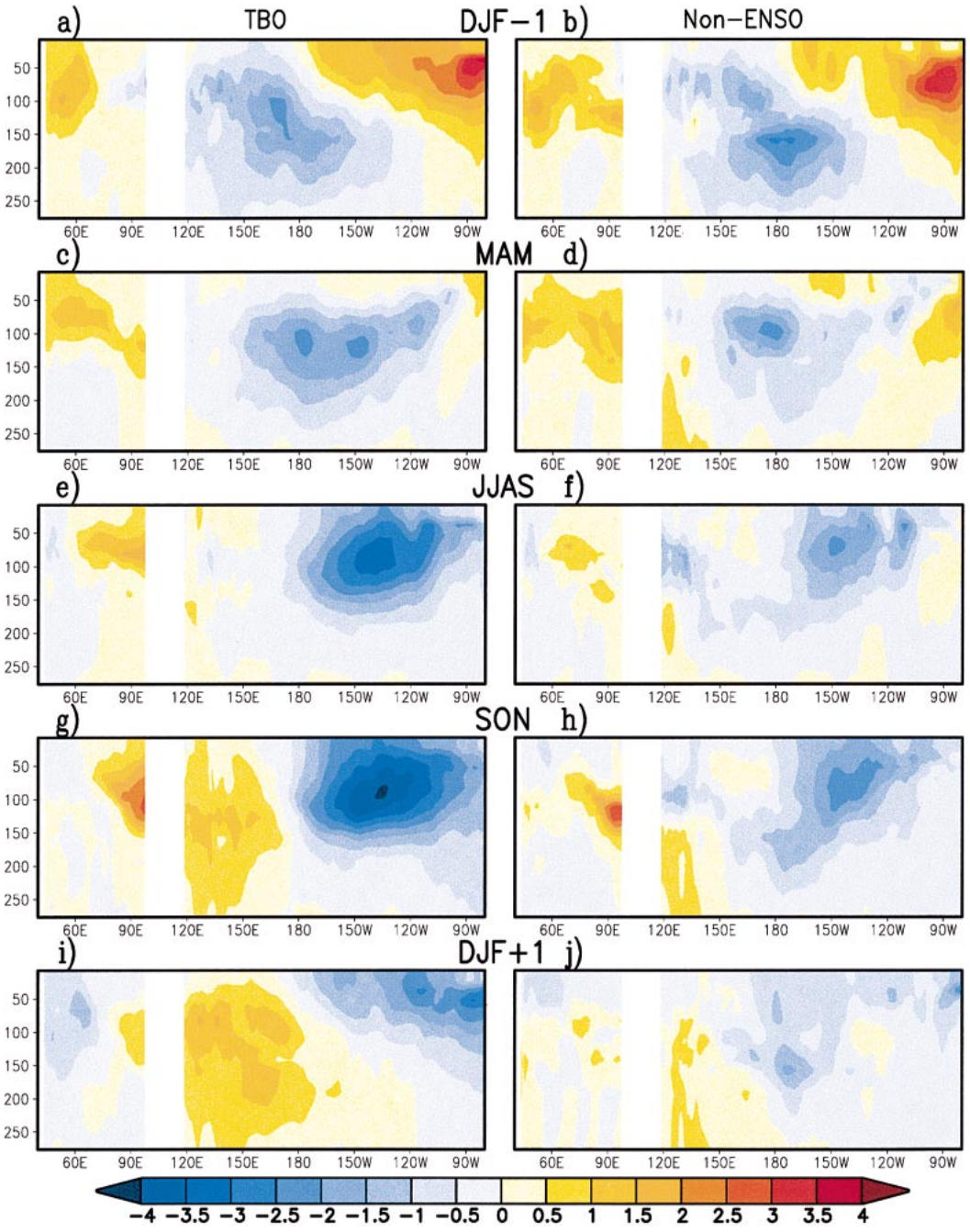

FIG. 9. As in Fig. 5, except for equatorial Indian and Pacific upper-ocean composite differences (°C) from the SODA ocean data (Carton et al. 2000a,b).

patterns to the all-TBO year composites except they have about half the magnitude.

With both the Indian basin and Pacific basin represented on the same plot, some interesting relationships emerge. In both basins, subsurface transitions in the TBO along the equator in seasons prior to and after a relatively strong Indian monsoon involve eastward-propagating temperature anomaly signals at the thermocline depth. In the Indian Ocean, positive temperature anomalies move eastward across the basin at the depth of the thermocline, while negative temperature anomalies move eastward at thermocline depth in the Pacific. Kelvin wave dynamics, associated with a collection of anomalous wind forcing events spread across a season, could be contributory factors in both basins. The relatively slow phase speed (discussed shortly in

relation to Fig. 10) suggests a collection of successive Kelvin waves or some kind of coupled propagating wave signal (e.g., Webster et al. 1999).

Wave dynamics in the Indian Ocean possibly tied to the patterns in Fig. 9 has been invoked by several previous studies. The observational study of Luyten and Roemmich (1982) deduced a mixture of an equatorial Kelvin wave and a long equatorial Rossby wave of the first meridional mode, with zonal wavelengths of 24 000 and 8000 km, respectively. The observed variations in zonal velocity in their study correspond to a period of 180 days. Jensen (1993) and Clarke and Liu (1993) suggest that resonant wind stress forcing can explain a strong semiannual response. They argue that the basin geometry allows for resonant forcing of the second baroclinic mode, with an excitation of equatorial Kelvin (Rossby) waves that traverse the Indian Ocean in 1.5 (4.5) months, reflect at the eastern (western) boundary, and transfer their energy to a westward (eastward) Rossby (Kelvin) wave. Similar wave dynamics in both the 26- and 180-day periods were present in the model of McCreary et al. (1993).

In any case, the western Walker cell in the Indian Ocean is associated with wind forcing (and thus possible Kelvin wave response) opposite in sign to those associated with the anomalous eastern Walker cell in the Pacific. Additionally, a dipole of SST anomalies or anomalous SST gradient exists in the Pacific for an entire year (JJAS, SON, DJF, and MAM) while such an SST dipole in the Indian Ocean only occurs for two seasons (JJAS and SON).

c. Indian Ocean heat content

To identify the possible ocean wave dynamics from signatures of ocean heat content, we plot Hovmoeller diagrams of monthly heat content anomalies in the upper 125 m of the Indian Ocean for composites of positive minus negative TBO years (top of Fig. 10) and the non-ENSO year composites (bottom). The latitude band 2°N–2°S is plotted to identify equatorial signals, and 11°–13°S for possible ocean Rossby waves [the latter following Webster et al. (1999)]. First for the equatorial sector at left, positive heat content anomalies of greater than 50°C m are present early in January–February of year 0 in association with the positive upper-ocean temperature anomalies in Fig. 9a. As the westerly anomaly winds set up in the western equatorial Indian Ocean in MAM (Fig. 2c), the positive heat content anomalies propagate across the basin to become established in the eastern Indian Ocean in late northern fall with values exceeding 225°C m. These heat content anomalies are associated with positive upper-ocean temperature anomalies in the upper 125 m in the eastern Indian Ocean in SON (Fig. 9g). As the westerly anomaly winds strengthen and spread across the basin with convergence into the anomalously strong convective maximum over southeast Asia from SON to DJF + 1 (Figs. 2g,i), the warm surface waters are advected eastward and cooler subsurface water is brought to the surface, which shallows the thermocline and contributes to negative ocean heat content anomalies moving across the basin from northern fall into the following northern spring in association with the cooling of upper-ocean temperatures in DJF + 1 (Fig. 9i). The movement of positive ocean heat content anomalies across the equatorial Indian Ocean, with a phase speed of about 0.24 m s^{-1} from northern spring to northern fall, is associated with the anomalous westerly wind forcing shown in Fig. 2. For the non-ENSO TBO years in Fig. 10c, there is a similar but lower-amplitude movement of positive ocean heat content anomalies across the Indian Ocean from northern spring to northern fall with a comparable phase speed. This phase speed is too slow for a single first-mode Kelvin wave, though a succession of Kelvin waves over the course of a season could result in a composite propagation speed as shown in Fig. 10. Such a slowly propagating signal could also indicate some type of coupled wave dynamics as well, though propagation at the equatorial Kelvin wave speed is not expected theoretically. At these latitudes, both Rossby and Kelvin waves, free and wind forced, contribute to the response. Depending on the structure of the wind forcing, propagation in either direction at any speed is possible.

Webster et al. (1999) showed a Hovmoeller diagram of Indian Ocean sea surface height anomalies for the period January 1997 to July 1998. Their plot for 11°–13°S showed negative anomalies propagating westward during northern spring of 1997 through northern fall of 1997. Those were replaced by a positive anomaly appearing near 100°E in July 1997, propagating westward to expand and intensify positive sea surface height anomalies by the following northern spring. They indicated this was evidence of ocean Rossby waves driven by surface wind anomalies. This was confirmed in a subsequent study by Xie et al. (2002) who showed wind-forced Rossby waves and associated SST anomalies at these latitudes in the southern Indian Ocean. This is also the case here. Plots of wind stress curl anomalies (not shown) indicate wind-forced upwelling across the Indian Ocean from about 10° to 20°S during SON and DJF + 1. Such coupled ocean dynamics contribute to the negative heat content and SST anomalies across the Indian Ocean south of the equator at those times as noted in Fig. 10. It has been postulated that the Indian Ocean dipole of SSTs could be a remnant of such a southern Indian Ocean Rossby wave (e.g., Xie et al. 2002). Additionally, the Rossby wave could reflect off the east coast of Africa into the equatorial waveguide and help maintain heat content anomalies there, though there does not seem to be a strong connection at the western boundary between the heat content signals in Figs. 10a,b. This weak reflection signal is consistent with results of Battisti (1989) and Kessler (1991), who show that Rossby waves this far from the equator are likely

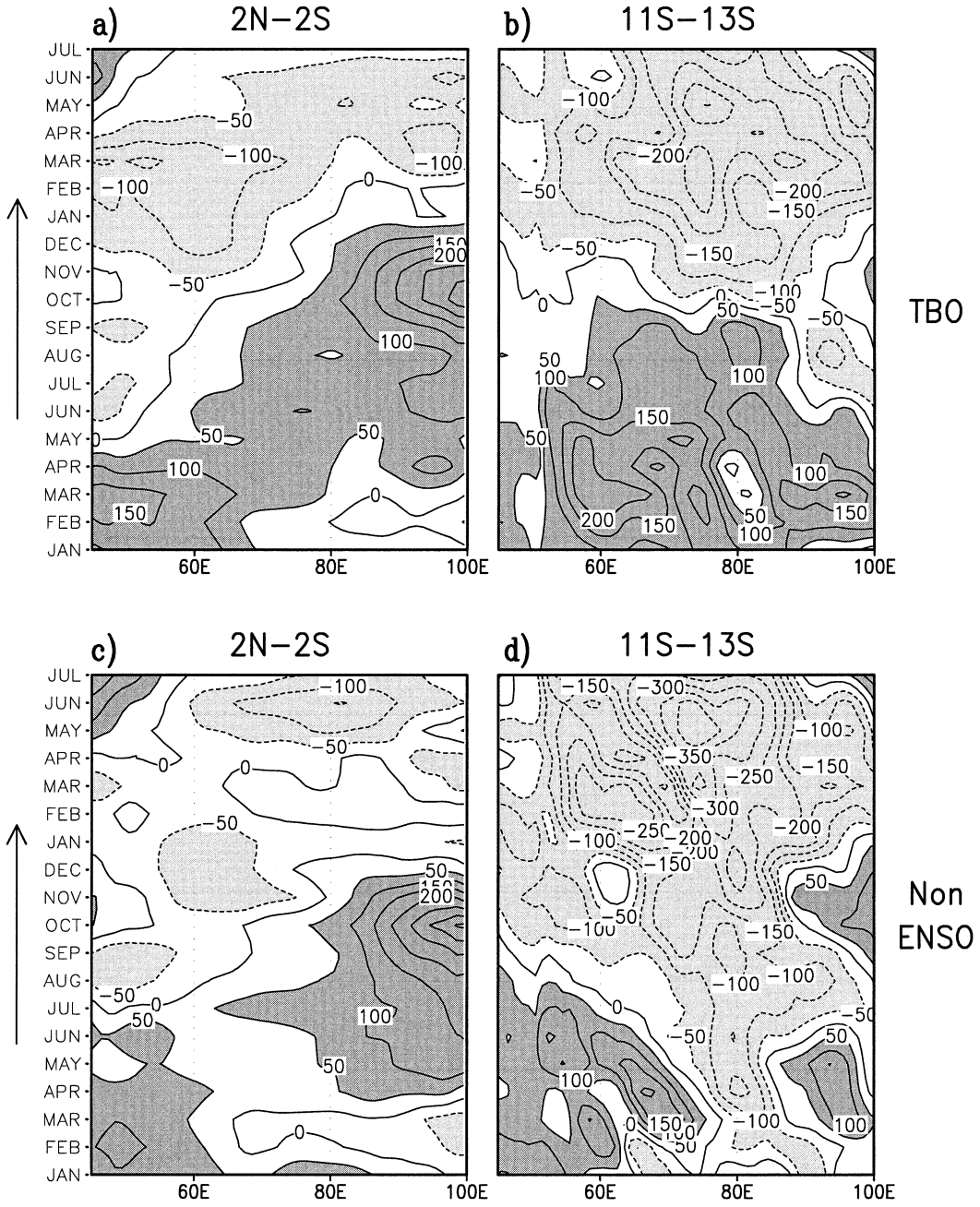

FIG. 10. Hovmoeller diagram of composite monthly heat content differences (°C m) calculated over the top 125 m of the Indian Ocean, positive minus negative TBO Indian monsoon years, time increasing upward starting with the Jan before a relatively strong Indian monsoon, running through the relatively strong Indian monsoon during northern summer, to the following northern winter, and ending with the following northern summer with a relatively weak Indian monsoon for (a) all TBO years, averaged 2°N–2°S; (b) all TBO years, averaged 11°–13°S; (c) non-ENSO onset TBO years, averaged 2°N–2°S; and (d) non-ENSO onset TBO years, averaged 2°N–2°S (calculated from the SODA ocean data; Carton et al. 2000a,b).

to contribute negligibly to signals in the equatorial wave guide.

A similar plot to the one in Webster et al. (1999) is shown for the TBO strong minus weak composites in Fig. 10b for all TBO years. The sign convention in this plot is opposite to the Webster et al. (1999) results since they were analyzing one year with a positive dipole (warm in the west, cold in the east). The sign convention of our composites is for a negative dipole (cold in the west, warm in the east). Nevertheless, the results from the composite in Fig. 10b also indicate that Rossby wave dynamics are contributing to the heat content anomalies in the western Indian Ocean. Positive values greater than 100°C m propagate westward starting at 100°E in late

DJF − 1 in Fig. 10b, with another maximum seen to propagate westward from about 60°–80°E farther west. These two maxima were also seen in the single year results (with opposite sign) from Webster et al. (1999)

Also comparable to the Webster et al. results is the negative heat content maximum with amplitude larger than −100°C m that appears in the far eastern Indian Ocean near 100°E around July and propagates westward, thus contributing to the negative heat content anomalies in the western Indian Ocean indicated by the negative temperature anomalies there in Figs. 9g,i in SON and DJF + 1, respectively. This indicates upwelling oceanic Rossby wave activity and consequent large negative heat content anomalies (over −250°C m near 90°E by the end of DJF + 1) that are part of the TBO mechanism. It involves the ocean retaining the memory of the coupled interactions of one year into the next via ocean heat content anomalies and consequent SST anomalies in some regions. These in turn affect convection, precipitation, and coupled interactions in the next TBO cycle.

The heat content anomalies at 11°–13°S for non-ENSO years in Fig. 10d actually have larger amplitude values than the composites in Fig. 10b for all TBO years. There is even clearer propagation of upwelling ocean Rossby waves with negative heat content signatures greater than −50°C m starting with January during the DJF-1 season from about 90°E, with the similar negative anomalies at 100°E during JJAS. These propagate westward with a phase speed of about 0.12 cm s^{-1} and contribute to the negative heat content anomalies in the western Indian Ocean with values ranging from greater than −100°C m to over −300°C m. It is interesting that in this particular composite of non-ENSO TBO years, compared to other such composites shown so far, the anomalies are actually greater. This is likely related to the fact that Meehl and Arblaster (2002a) showed that the Indian Ocean SST SVD relationship with Indian monsoon rainfall had greater amplitude in the central and southern Indian Ocean. This suggests a difference in the strength of the coupled interactions in that region during non-ENSO TBO years, and is currently under study. However, for the purposes of the present analysis, the net result is the same in contributing to ocean heat content changes that, in most cases, are associated with comparable SST anomalies [e.g., comparing to Fig. 2, and noted by Xie et al. (2002)]. These carry over to the next year as the memory of the coupled interactions of the previous year, an integral element of the TBO mechanism.

d. Indian Ocean heat transport

W2003 and Loschnigg and Webster (2000) have shown that cross-equatorial heat transport driven by anomalous surface winds contributes to regulating SST anomalies in the Indian Ocean related to monsoon strength. Loschnigg et al. (2003) analyzed the NCAR Climate System Model (CSM), a global coupled climate model, to show that anomalous southward heat transport anomalies contributed to negative heat content and SST anomalies in the tropical Indian Ocean as part of the TBO in the model. Here we perform a similar calculation to show the role of cross-equatorial heat transport in the TBO in the observations.

Anomalous westerlies between the equator and 10°N and easterlies in the southeast Indian Ocean in JJAS (Fig. 2e) should produce anomalous southward heat transport. This was postulated by Loschnigg and Webster (2000) and W2003 to contribute to negative heat content anomalies becoming established there in northern fall. Calculation of composite anomalous heat transport zonally averaged from 5°N to the equator (indicative of cross-equatorial heat transport, as shown, e.g., for the NCAR coupled model in Loschnigg et al. 2003) for positive minus negative TBO years for JJAS from the SODA ocean data is slightly negative or southward with a value of −0.01 PW (1 PW = 1×10^{15} W). The climatological value for heat transport (1950–99 from the SODA data) for this latitudinal band for JJAS is −1.30 PW. For the latitudinal band averaged from 10° to 15°S the anomalous southward heat transport for JJAS is larger with a value of −0.13 PW (or an increase of southward heat transport of 7% compared to the climatological value of −1.88 PW) and becomes even larger for the SON season at 11% (an anomaly of −0.14 PW compared to a climatological value of −1.32 PW).

As indicated earlier, the pattern for the non-ENSO onset years indicates stronger cooling of SSTs in the Indian Ocean north of the equator in JJAS. This is associated with greater magnitude anomalous southward cross-equatorial heat transport for the latitude band 5°N to the equator for positive minus negative non-ENSO onset TBO years during JJAS with a value of −0.22 PW or 17%. For the band 10°–15°S the anomalous southward heat transport for JJAS is −0.21 PW or 11% for non-ENSO onset TBO years, and rises to −0.29 PW (22%) in SON. Thus, consistent with previous studies of Loschnigg and Webster (2000), W2003, and Miyama et al. (2003), anomalous wind forcing can produce anomalous ocean heat transport that can contribute to changing heat content and SSTs in the Indian Ocean. Results here show that for JJAS for both all-TBO years and non-ENSO onset TBO years there is anomalous southward heat transport near the equator with larger values near 10°–15°S, and larger-amplitude anomalies for the non-ENSO onset TBO years. That is, for a strong Indian monsoon and subsequent strong convective maximum traversing from south Asia toward northern Australia, there is anomalous southward ocean heat transport out of the equatorial Indian Ocean that contributes to reducing upper-ocean heat content and lowering SSTs there.

5. Synthesis of TBO coupled interactions

To provide a synthesis of the TBO cycle in the context of the results presented in this paper, we construct plots

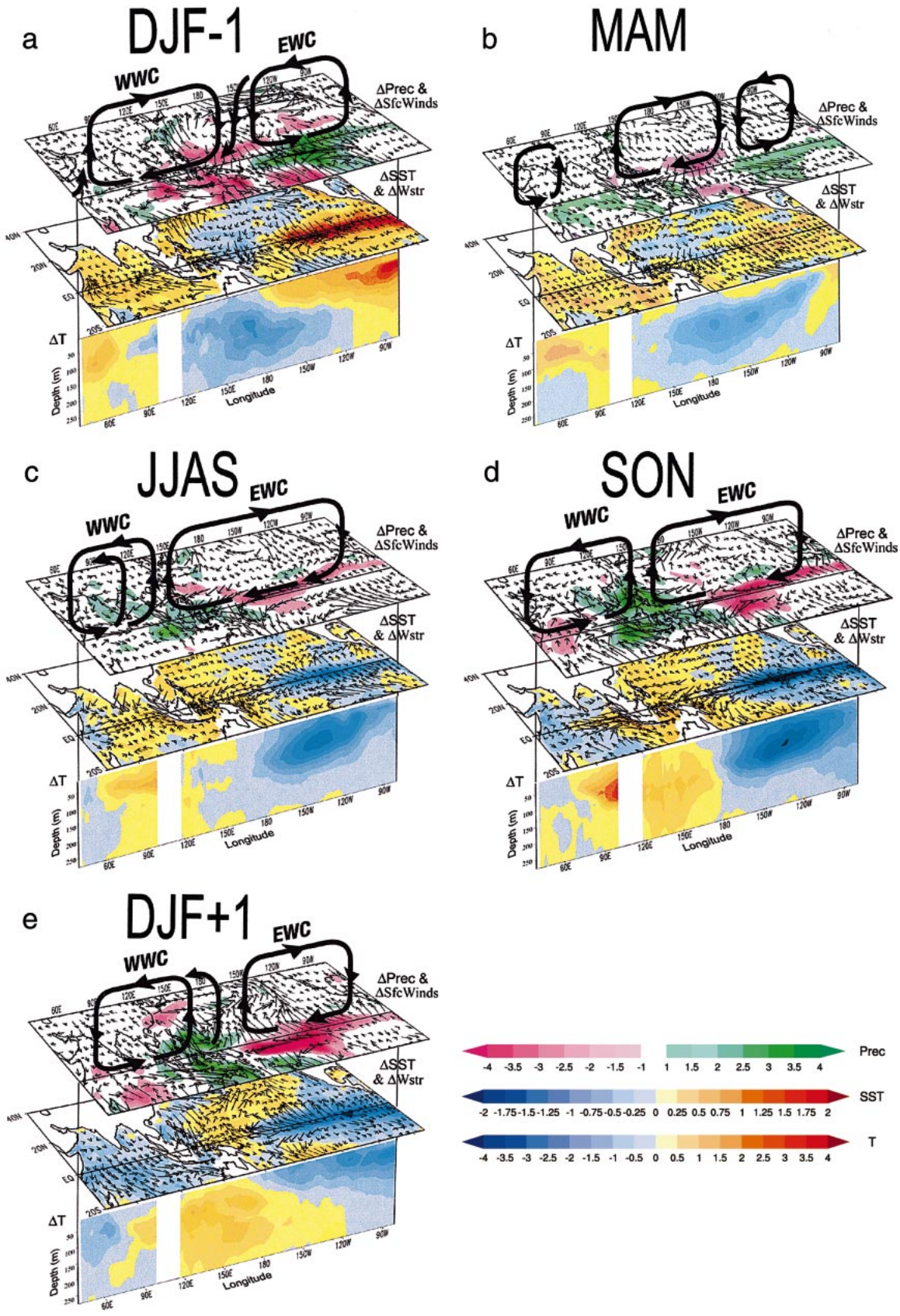
a
DJF-1
WWC
EWC
ΔPrec &
ΔSfcWinds
ΔSST
& ΔWstr
ΔT
Depth (m)
Longitude
b
MAM
c
JJAS
d
SON
e
DJF+1
Prec
-4 -3.5 -3 -2.5 -2 -1.5 -1 1 1.5 2 2.5 3 3.5 4
SST
-2 -1.75 -1.5 -1.25 -1 -0.75 -0.5 -0.25 0 0.25 0.5 0.75 1 1.25 1.5 1.75 2
T
-4 -3.5 -3 -2.5 -2 -1.5 -1 -0.5 0 0.5 1 1.5 2 2.5 3 3.5 4

in Fig. 11 that include strong minus weak TBO year composites of equatorial ocean temperature anomalies at the bottom of each panel (comparable to Fig. 9, left); SST (after Fig. 2) and surface wind stress anomalies in the middle; precipitation and surface wind anomalies (from Fig. 2, left) at top; and a schematic representation of the omega anomaly composites (Fig. 4, left) indicative of Walker circulation anomalies above. Additionally, we show surface wind stress anomalies superimposed on the SST anomalies.

In the DJF season prior to a strong Indian monsoon (Fig. 11a) there is a relatively weak Australian monsoon (negative precipitation anomalies over the northern Australian and Indonesian regions), warm SST and upper-ocean temperature anomalies to the west in the Indian Ocean and to the east in the central and eastern Pacific, and relatively cool SSTs and negative subsurface ocean temperature anomalies north of Australia. At the surface there are anomalous easterly surface winds and surface wind stress in the southeastern tropical Indian and far western Pacific indicative of the weak Australian monsoon flow. This is associated with weak western and eastern Walker cells indicated by anomalous subsidence over the Australian monsoon and ascent over the western Indian Ocean and eastern Pacific. Southeasterly offshore winds off the west coast of Sumatra are associated with negative subsurface temperature anomalies in the eastern equatorial Indian Ocean indicative of anomalous upwelling there. Positive SST anomalies near 11°–13°S in the Indian Ocean are associated, for the most part, with the positive heat content anomalies in the region in Fig. 10b.

The anomalous easterly winds in the western Pacific could induce eastward-propagating upwelling Kelvin waves in the ocean, though both wind-forced and free Kelvin and Rossby waves contribute to the equatorial response. The result is the eastward spread of negative subsurface temperature anomalies near 100 m as the thermocline is raised in the central and eastern Pacific during MAM as shown in Fig. 11b. Meanwhile, in the far western Indian Ocean, there are westerly anomaly surface winds and surface wind stresses near the anomalous convection over the western Indian Ocean. The wind forcing moves warm surface water eastward and brings cooler water to the surface. This produces anomalous upwelling and a shallower thermocline in the west, and a possible collection of downwelling Kelvin waves that could contribute to a deepening of the thermocline (positive subsurface temperature anomalies across the equatorial Indian Ocean from 50–100 m) and positive equatorial heat content anomalies propagating across the basin from DJF − 1 to JJAS (Fig. 10a).

Upwelling Kelvin waves from the easterly anomaly winds and surface wind stresses in the western Pacific during DJF, continuing into MAM, in addition to possible contributions from western and eastern ocean boundary reflection of Kelvin and Rossby waves, could contribute to raising the thermocline in the central and eastern Pacific and provide the conditions for a change in sign or transition of SST anomalies in the eastern Pacific from positive in MAM (Fig. 11b) to negative in JJAS (Fig. 11c). Additionally, zonal advection in the central Pacific could also play a role (McPhaden and Picaut 1990; Picaut et al. 1997; Shu and Clarke 2002; Wang and McPhaden 2000).

Small-amplitude easterly surface winds in the equatorial eastern Pacific bring the cooler subsurface water to the surface (Fig. 11c). In the Indian Ocean, westerly anomaly winds along the equator associated with stronger convection in the eastern Indian Ocean raise the thermocline in the west through enhanced upwelling (negative subsurface temperature anomalies) and lower it in the east (positive subsurface temperature anomalies, with possible contributions from downwelling Kelvin waves). Also during JJAS (Fig. 11c), convection and precipitation over the Indian monsoon region are strong (note in this view of the monsoon, land and ocean precipitation are included over a broad area of south Asia, the tropical Indian Ocean, and extending to southeast Asia, the sum of which are presumed to be dynamically important for the coupled interactions involved with the TBO). The sense of the Walker circulation has reversed from DJF − 1. The strong monsoon convection is associated with anomalous upward motion, downward motion over the western Indian Ocean in the western Walker cell, and subsidence over the eastern Pacific in the eastern Walker cell. Easterly anomaly surface winds and wind stresses in the southeast Indian Ocean near 13°S along with the westerly anomaly winds and wind stresses near the equator produce an upwelling Rossby wave during JJAS that propagates westward with a signature of negative heat content anomalies (see Fig. 10b).

The SON season after the strong Indian monsoon (Fig. 11d) is characterized by a strong convective max-

←

FIG. 11. Time sequence of TBO evolution showing positive minus negative TBO composites for equatorial upper-ocean temperature differences (°C), SST (°C), surface wind stress (scaling arrow = 0.03 N m^{-2}), precipitation (mm day^{-1}), surface winds (scaling arrow = 1.0 m s^{-1}), and schematic representation of large-scale Walker circulation anomalies (WWC = western Walker cell, EWC = eastern Walker cell) for (a) DJF − 1 showing the weak Australian monsoon prior to a strong Indian monsoon, (b) the MAM season before a strong Indian monsoon, (c) strong Indian monsoon season during JJAS, (d) SON season after a strong Indian monsoon and prior to a strong Australian monsoon, and (e) strong Australian monsoon following a strong Indian monsoon. Contour interval for precipitation is 0.5 mm day^{-1} (values between −1 and +1 mm day^{-1} are not plotted), for SST is 0.25°C, and for upper-ocean temperature is 0.5°C. Comparable depictions of precipitation and surface winds are given in Fig. 2. SST anomalies are from the SODA data and are very similar to the NCEP–NCAR SSTs in Fig. 2. Wind stress anomalies are from the NCEP–NCAR reanalyses, and upper-ocean temperature anomalies are taken from Fig. 9.

imum (positive precipitation anomalies) traversing with the seasonal cycle over Southeast Asia, being reinforced by enhanced evaporation from warm SSTs set up by the dynamical ocean response to the westerly anomaly winds and wind stresses in the western equatorial Indian Ocean during the previous season. There is a negative dipole of SST anomalies (anomalous SST gradient) across the Indian Ocean that is a natural consequence of TBO evolution. The tropical Pacific has negative SST and subsurface temperature anomalies in the eastern equatorial Pacific in Fig. 11d (a La Niña event in the extreme). The large-scale east–west atmospheric circulation shows both an anomalously strong western Walker cell (westerly anomaly surface winds and wind stresses across the Indian Ocean) and eastern Walker cell (easterly anomaly surface winds and wind stresses across the Pacific Ocean). Negative SST anomalies in the western and southwestern tropical Indian Ocean are associated with anomalous upwelling and negative subsurface temperature anomalies in the equatorial western Indian Ocean, as well as upwelling Rossby wave activity forced by the combination of westerly anomaly winds near the equator and easterly component anomaly winds and wind stresses near 13°S. This is evidenced by the propagation of negative heat content anomalies westward at 11°–13°S in the Indian Ocean (see Fig. 10b).

In the western equatorial Pacific in SON (Fig. 11d), positive subsurface temperature anomalies are indicative, for the most part, of a deepening thermocline associated with anomalously warm SSTs. This sets up increased evaporation and, thus, an enhanced moisture source for the subsequent strong Australian monsoon (positive precipitation anomalies over the Australian monsoon domain of northern Australia, Indonesia, and parts of Malaysia) in DJF + 1 (Fig. 11e). The strong western Walker cell is associated with westerly anomaly surface winds and wind stresses across the Indian Ocean and particularly in the southeast Indian Ocean in association with strong inflow into the Australian monsoon. The eastern Walker cell is also strong, with anomalous easterlies across the Pacific (Fig. 11e). SSTs in the Indian Ocean have now completed the transition from mostly warm SST anomalies the previous DJF to mostly cool in Fig. 11e. But anomalous westerlies in the far western equatorial Pacific associated with strong convection start to set off downwelling equatorial oceanic Kelvin waves that deepen the thermocline to the east as indicated by the eastward spread of positive upper-ocean temperature anomalies at the depth of the thermocline west of 120°W. This sets up the next transition to warm SSTs in the central and eastern equatorial Pacific the following MAM–JJAS. This composite TBO sequence follows, with opposite signs, to the following MAM, culminating in a weak Indian monsoon the following JJAS (not shown).

6. Conclusions

Composite analyses of years associated with TBO transitions have confirmed earlier SVD analyses in that the Indian and Pacific Ocean SST anomalies play a large role in TBO variability. Meridional temperature gradients over Asia, though important in some years as shown by the previous SVD and pattern correlation analyses, are likely of secondary importance since they do not show up strongly in the composites. The linkage of the strong Indian monsoon to strong Australian monsoon is seen as the establishment of the large-scale east–west atmospheric circulation with the eastern Walker cell linking Asian–Australian monsoon precipitation anomalies with coupled dynamics in the Pacific, and the western Walker cell tying Asian–Australian monsoon precipitation anomalies to coupled dynamical processes in the Indian Ocean. Thus, the monsoon convective maximum that traverses south Asia from the Indian monsoon in JJAS to the Australian monsoon in DJF is the common element that links coupled dynamics in the tropical Indian and Pacific Oceans. This southeastward movement of the convective maximum from the Indian monsoon region to the Australian monsoon, encountering SST anomalies en route set up the previous year by coupled precipitation–wind–ocean dynamical processes, produces an Indian Ocean SST dipole (anomalous SST gradient or zonal mode) with a maximum in SON as consequence of the evolution of the coupled convection–wind–dynamical ocean response involved with the TBO. Rao et al. (2002) have also noted the role of such ocean dynamical mechanisms in contributing to transitions of the dipole pattern of Indian Ocean SSTs.

An essential element of the TBO mechanism is the memory of the ocean. That is, the upper ocean must retain heat content anomalies and associated SST anomalies against dissipation from one year to the next. We have confirmed previous studies (e.g., Webster et al. 1999; Loschnigg and Webster 2000; W2003) and shown the important function of coupled ocean dynamics in contributing to this memory involved with the TBO. In particular, equatorial Kelvin waves in the Indian and Pacific Oceans are likely to contribute to the observed changes in the depth of the thermocline and set the stage for transitions of SSTs, as well as produce heat content anomalies that contribute to maintaining SST anomalies for several seasons after they are set up. In addition, previously postulated Rossby wave dynamics south of the equator in the Indian Ocean also are shown to play a role in setting up heat content and SST anomalies in the southwest and western Indian Ocean. Finally, cross-equatorial heat transport forced by anomalous winds also contributes to heat content and SST anomalies in the Indian Ocean.

In this way, coupled dynamical interactions involving atmosphere and ocean sustain the TBO interannual transitions, with the phasing of the transitions in each ocean dependent on the seasonal cycle of convection in the respective regions. Thus, the anomalously weak Australian monsoon rainfall in DJF and associated surface wind anomalies in the far western equatorial Pacific could trigger oceanic Kelvin waves that contribute to

the Pacific SST transition a season later in MAM. Likewise, anomalous monsoon rainfall and associated surface wind anomalies in the tropical Indian Ocean during JJAS contribute to the Indian Ocean SST dipole (zonal mode, or anomalous SST gradient) appearing in JJAS and SON, transitioning to SST anomalies of all one sign by DJF in association with the anomalous surface wind forcing connected with the Australian monsoon to the east. Simultaneously, surface wind anomalies to the east of the Australian monsoon in the far western equatorial Pacific then start acting on the Pacific Ocean to initiate the subsequent transition there in MAM, and so on. Therefore, the coupled SST transitions in the Indian Ocean do not occur simultaneously with those in the Pacific, but they are linked through the evolution of Asian–Australian monsoon convective maximum via the western and eastern Walker cells.

Previous studies have pointed to the role of surface wind forcing in the western equatorial Pacific (Lau and Wu 1999, 2001; Kim and Lau 2001; Clarke et al. 1998; Clarke and Shu 2000; Chung and Nigam 1999) and equatorial Indian Ocean (Clarke et al. 1998; Reason et al. 2000; Saji et al. 1999; Webster et al. 1999; Hendon 2003). Here we place these forcings in the framework of the TBO evolution involving dynamic coupled interactions across the Indian and Pacific sectors. The upper-ocean heat content anomalies that are a consequence contribute to the persistence of SST anomalies that are crucial for the convective heating anomalies and maintenance of the large-scale east–west circulation in the atmosphere involving both the eastern and western Walker cells during the TBO in Indian and Pacific Oceans.

Acknowledgments. A portion of this study was supported by the Office of Biological and Environmental Research, U.S. Department of Energy, as part of its Climate Change Prediction Program.

REFERENCES

Allan, R. J., and R. D. D'Arrigo, 1999: ''Persistent'' ENSO sequences: How unusual was the 1990–95 El Niño? *Holocene,* **9,** 101–118.

Ashok, K., Z. Guan, and T. Yamagata, 2001: Impact of the Indian Ocean dipole on the relationship between the Indian monsoon rainfall and ENSO. *Geophys. Res. Lett.,* **28,** 4499–4502.

Battisti, D. S., 1989: On the role of off-equatorial oceanic Rossby waves during ENSO. *J. Phys. Oceanogr.,* **19,** 551–560.

Brier, G. W., 1978: The quasi-biennial oscillation and feedback processes in the atmosphere–ocean–earth system. *Mon. Wea. Rev.,* **106,** 938–946.

Carton, J. A., G. Chepurin, and X. Cao, 2000a: A Simple Ocean Data Assimilation analysis of the global upper ocean 1950–1995. Part 2: Results. *J. Phys. Oceanogr.,* **30,** 311–326.

——, ——, ——, and B. S. Giese, 2000b: A Simple Ocean Data Assimilation analysis of the global upper ocean 1950–1995. Part 1: Methodology. *J. Phys. Oceanogr.,* **30,** 294–309.

Chang, C. P., and T. Li, 2000: A theory for the tropical tropospheric biennial oscillation. *J. Atmos. Sci.,* **57,** 2209–2224.

Chung, C., and S. Nigam, 1999: Asian summer monsoon–ENSO feedback on the Cane–Zebiak model ENSO. *J. Climate,* **12,** 2787–2807.

Clark, C. O., J. E. Cole, and P. J. Webster, 2000: Indian Ocean SST and Indian summer rainfall: Predictive relationships and their decadal variability. *J. Climate,* **13,** 2503–2519.

Clarke, A. J., 1994: Why are surface equatorial ENSO winds anomalously westerly under anomalous large-scale convection? *J. Climate,* **7,** 1623–1632.

——, and X. Liu, 1993: Observations and dynamics of semiannual and annual sea levels near the eastern equatorial Indian Ocean boundary. *J. Phys. Oceanogr.,* **23,** 386–399.

——, and L. Shu, 2000: Quasi-biennial winds in the far western equatorial Pacific phase-locking El Niño to the seasonal cycle. *Geophys. Res. Lett.,* **27,** 771–774.

——, X. Liu, and S. van Gorder, 1998: Dynamics of the biennial oscillation in the equatorial Indian and far western Pacific Oceans. *J. Climate,* **11,** 987–1001.

Hendon, H. H., 2003: Indonesian rainfall variability: Impacts of ENSO and local air–sea interaction. *J. Climate,* **16,** 1775–1790.

Iizuka, S., T. Matsuura, and T. Yamagata, 2000: The Indian Ocean SST dipole simulated in a coupled general circulation model. *Geophys. Res. Lett.,* **27,** 3369–3372.

Jensen, T., 1993: Equatorial variability and resonance in a wind-driven Indian Ocean model. *J. Geophys. Res.,* **98,** 22 533–22 552.

Ji, M., A. Kumar, and A. Leetmaa, 1994: A multiseason climate forecast system at the National Meteorological Center. *Bull. Amer. Meteor. Soc.,* **75,** 569–577.

——, A. Leetmaa, and J. Derber, 1995: An ocean analysis system for seasonal to interannual climate studies. *Mon. Wea. Rev.,* **123,** 460–481.

Kalnay, E., and Coauthors, 1996: The NCEP/NCAR Reanalysis Project. *Bull. Amer. Meteor. Soc.,* **77,** 437–471.

Kessler, W., 1990: Observation of long Rossby waves in the northern tropical Pacific. *J. Geophys. Res.,* **95,** 5183–5217.

——, 1991: Can reflected extra-equatorial Rossby waves drive ENSO? *J. Phys. Oceanogr.,* **21,** 444–452.

Kiladis, G. N., and H. van Loon, 1988: The Southern Oscillation. Part VII: Meteorological anomalies over the Indian and Pacific sectors associated with the extremes of the oscillation. *Mon. Wea. Rev.,* **116,** 120–136.

——, and H. F. Diaz, 1989: Global climatic anomalies associated with extremes in the Southern Oscillation. *J. Climate,* **2,** 1069–1090.

Kim, K.-M., and K.-M. Lau, 2001: Dynamics of monsoon-induced biennial variability in ENSO. *Geophys. Res. Lett.,* **28,** 315–318.

Kumar, K. K., B. Rajagopalan, and M. A. Cane, 1999: On the weakening relationship between the Indian monsoon and ENSO. *Science,* **284,** 2156–2159.

Lau, K. M., and H.-T. Wu, 1999: Assessment of the impacts of the 1997–98 El Niño on the Asian-Australia monsoon. *Geophys. Res. Lett.,* **26,** 1747–1750.

——, and ——, 2001: Principal modes of rainfall-SST variability of the Asian summer monsoon: A re-assessment of monsoon–ENSO relationships. *J. Climate,* **14,** 2880–2895.

Li, T., C.-W. Tham, and C.-P. Chang, 2001a: A coupled air–sea–monsoon oscillator for the tropospheric biennial oscillation. *J. Climate,* **14,** 752–764.

——, Y. Zhang, C.-P. Chang, and B. Wang, 2001b: On the relationship between Indian Ocean sea surface temperature and Asian summer monsoon. *Geophys. Res. Lett.,* **28,** 2843–2846.

Loschnigg, J., and P. J. Webster, 2000: A coupled ocean–atmosphere system of SST modulation for the Indian Ocean. *J. Climate,* **13,** 3342–3360.

——, G. A. Meehl, J. M. Arblaster, G. P. Compo, and P. J. Webster, 2003: The Asian monsoon, the tropospheric biennial oscillation, and the Indian Ocean dipole in the NCAR CSM. *J. Climate,* **16,** 1617–1642.

Luyten, J. R., and D. H. Roemmich, 1982: Equatorial currents at semi-annual period in the Indian Ocean. *J. Phys. Oceanogr.,* **12,** 406–413.

McCreary, J. P., Jr., P. K. Kundu, and R. L. Molinari, 1993: A numerical investigation of dynamics, thermodynamics and mixed-layer processes in the Indian Ocean. *Progress in Oceanography,* Vol. 31, Pergamon, 181–244.

McPhaden, M. J., and J. Picaut, 1990: El Niño–Southern Oscillation displacements of the western equatorial Pacific warm pool. *Science,* **250,** 1385–1388.

Meehl, G. A., 1987: The annual cycle and interannual variability in the tropical Indian and Pacific Ocean regions. *Mon. Wea. Rev.,* **115,** 27–50.

——, 1993: A coupled air–sea biennial mechanism in the tropical Indian and Pacific regions: Role of the ocean. *J. Climate,* **6,** 31–41.

——, 1994: Coupled land–ocean–atmosphere processes and south Asian monsoon variability. *Science,* **266,** 263–267.

——, 1997: The south Asian monsoon and the tropospheric biennial oscillation. *J. Climate,* **10,** 1921–1943.

——, and J. M. Arblaster, 2001: The tropospheric biennial oscillation and Indian monsoon rainfall. *Geophys. Res. Lett.,* **28,** 1731–1734.

——, and ——, 2002a: The tropospheric biennial oscillation and Asian–Australian monsoon rainfall. *J. Climate,* **15,** 722–744.

——, and ——, 2002b: Indian monsoon GCM experiments testing tropospheric biennial oscillation transition conditions. *J. Climate,* **15,** 923–944.

Meinen, C., and M. J. McPhaden, 2000: Observations of warm water volume changes in the equatorial Pacific and their relationship to El Niño and La Niña. *J. Climate,* **13,** 3551–3559.

Meyers, G., and L. Pigot, 1999: Analysis of frequently repeated XBT lines in the Indian Ocean. CSIRO Rep. 238, 43 pp. [Available from CSIRO Marine Laboratories, GPO 1538, Hobart, TAS 7008, Australia.]

Miyama, T., J. McCreary, T. G. Jenson, J. Loschnigg, S. Godfrey, and A. Ishida, 2003: Structure and dynamics of the Indian Ocean cross-equatorial cell. *Deep-Sea Res.,* in press.

Nicholls, N., 1978: Air–sea interaction and the quasi-biennial oscillation. *Mon. Wea. Rev.,* **106,** 1505–1508.

——, 2001: The insignificance of significance testing. *Bull. Amer. Meteor. Soc.,* **82,** 981–986.

Picaut, J., F. Masia, and Y. du Penhoat, 1997: An advective-reflective conceptual model for the oscillatory nature of the ENSO. *Science,* **277,** 663–666.

Rao, S. A., S. K. Behera, Y. Masumoto, and T. Yamagata, 2002: Interannual subsurface variability in the tropical Indian Ocean with a special emphasis on the Indian Ocean dipole. *Deep-Sea Res. II,* **49,** 1549–1572.

Reason, C. J. C., R. J. Allan, J. A. Lindesay, and T. J. Ansell, 2000: ENSO and climatic signals across the Indian Ocean basin in the global context: Part 1. Interannual composite patterns. *Int. J. Climatol.,* **20,** 1285–1327.

Saji, N. H., and T. Yamagata, 2003: Structure of SST and surface wind variability during Indian Ocean dipole events: COADS observations. *J. Climate,* in press.

——, B. N. Goswami, P. N. Vinayachandran, and T. Yamagata, 1999: A dipole mode in the tropical Indian Ocean. *Nature,* **401,** 360–363.

Shu, L., and A. J. Clarke, 2002: Using an ocean model to examine ENSO dynamics. *J. Phys. Oceanogr.,* **32,** 903–923.

Shukla, J., and D. A. Paolino, 1983: The Southern Oscillation and long-range forecasting of the summer monsoon rainfall over India. *Mon. Wea. Rev.,* **111,** 1830–1837.

Torrence, C., and P. J. Webster, 1999: Interdecadal changes in the ENSO–monsoon system. *J. Climate,* **12,** 2679–2690.

Trenberth, K. E., D. P. Stepaniak, and J. W. Hurrell, 2001: Quality of reanalyses in the Tropics. *J. Climate,* **14,** 1499–1510.

van Loon, H., 1986: The characteristics of sea level pressure and sea surface temperature during the development of a warm event in the Southern Oscillation. *Namias Symposium,* J. Roads, Ed., Scripps Institution of Oceanography, 160–173.

Vinayachandran, P. N., S. Iizuka, and T. Yamagata, 2002: Indian Ocean dipole mode events in an ocean general circulation model. *Deep-Sea Res.,* **49,** 1573–1596.

Wang, W., and M. J. McPhaden, 2000: The surface-layer heat balance in the equatorial Pacific Ocean. Part II: Interannual variability. *J. Phys. Oceanogr.,* **30,** 2989–3008.

Webster, P. J., and S. Yang, 1992: Monsoon and ENSO: Selectively interactive systems. *Quart. J. Roy. Meteor. Soc.,* **118,** 877–926.

——, V. O. Magana, T. N. Palmer, J. Shukla, R. A. Tomas, M. Yanai, and T. Yasunari, 1998: Monsoons: Processes, predictability, and the prospects for prediction. *J. Geophys. Res.,* **103,** 14 451–14 510.

——, A. M. Moore, J. P. Loschnigg, and R. R. Leben, 1999: Coupled ocean–atmosphere dynamics in the Indian Ocean during 1997–98. *Nature,* **401,** 356–360.

Xie, P., and P. A. Arkin, 1996: Analyses of global monthly precipitation using gauge observations, satellite estimates, and numerical model predictions. *J. Climate,* **9,** 840–858.

Xie, S.-P., H. Annamalai, F. A. Schott, and J. P. McCreary Jr., 2002: Structure and mechanisms of south Indian Ocean climate variability. *J. Climate,* **15,** 864–878.

Yasunari, T., 1990: Impact of Indian monsoon on the coupled atmosphere/ocean system in the tropical Pacific. *Meteor. Atmos. Phys.,* **44,** 29–41.